mice, calcified area appeared at postoperative week (POW) 1, and formed a bony bridge by POW 3. The volume of the fracture callus peaked at around POW 4 and subsequently decreased in size (Fig. 1B), whereas in *Stat1*$^{-/-}$ mice, the volume of the fracture callus peaked at around POW 3 and decreased at a higher rate than in wild-type mice, indicating that the fracture healing process is accelerated in STAT1-deficient environment. The cross-sectional callus area of the fracture site was significantly smaller in *Stat1*$^{-/-}$ mice compared with wild-type animals (0.76 ± 0.19 mm^2 in *Stat1*$^{-/-}$ mice and 1.72 ± 0.60 mm^2 in wild-type mice at POW 6, respectively; Fig. 1B), indicating that the callus resorption and bone remodeling is accelerated in the lack of STAT1 activity.

Rapid Turnover of Calcified Callus in *Stat1*$^{-/-}$ Mice

To examine how the lack of STAT1 affects the formation and resorption of callus and subsequent remodeling process in bone fracture healing, the tibiae from wild-type and *Stat1*$^{-/-}$ mice were harvested and histologically analyzed (Fig. 1C). In both genotypes, fractured bone was bridged by cartilage callus by POW 2 with no apparent differences in the volume of the cartilaginous tissue. The cartilage callus became fully calcified by POW 4 in both wild-type and *Stat1*$^{-/-}$ mice; however, the following remodeling process (i.e., resorption of calcified callus and subsequent bone formation) was highly accelerated in *Stat1*$^{-/-}$ mice compared with wild-type mice. These findings suggest that the lack of STAT1 activity during fracture healing results in accelerated callus remodeling, but has little effect in the inflammation phase or in the subsequent cartilage callus formation.

Membranous Ossification Is Accelerated in *Stat1*$^{-/-}$ Mice during Fracture Healing

The findings in the tibial fracture model experiments indicated that the lack of STAT1 leads to activation of both calcified callus resorption by osteoclasts and bone formation by osteoblasts. Although upregulation in osteoclast activity was clearly illustrated by faster disappearance of calcified callus, it was still unclear whether bone formation was also upregulated in the remodeling phase. To further evaluate the activity of osteoblasts during fracture healing; we next utilized a cortical defect model. In normal fracture healing, both enchondral ossification (characterized by transient cartilage formation followed by the bone formation on the cartilage template) and membranous ossification (characterized by bone formation by osteoblasts without cartilage formation) are usually observed. However, in this experimental model, skeletal healing is achieved without cartilage callus formation or resorption of calcified callus by osteoclasts so that membranous ossification by osteoblasts can solely be assessed.[9] As shown in Figure 2A and B, we found that bone formation

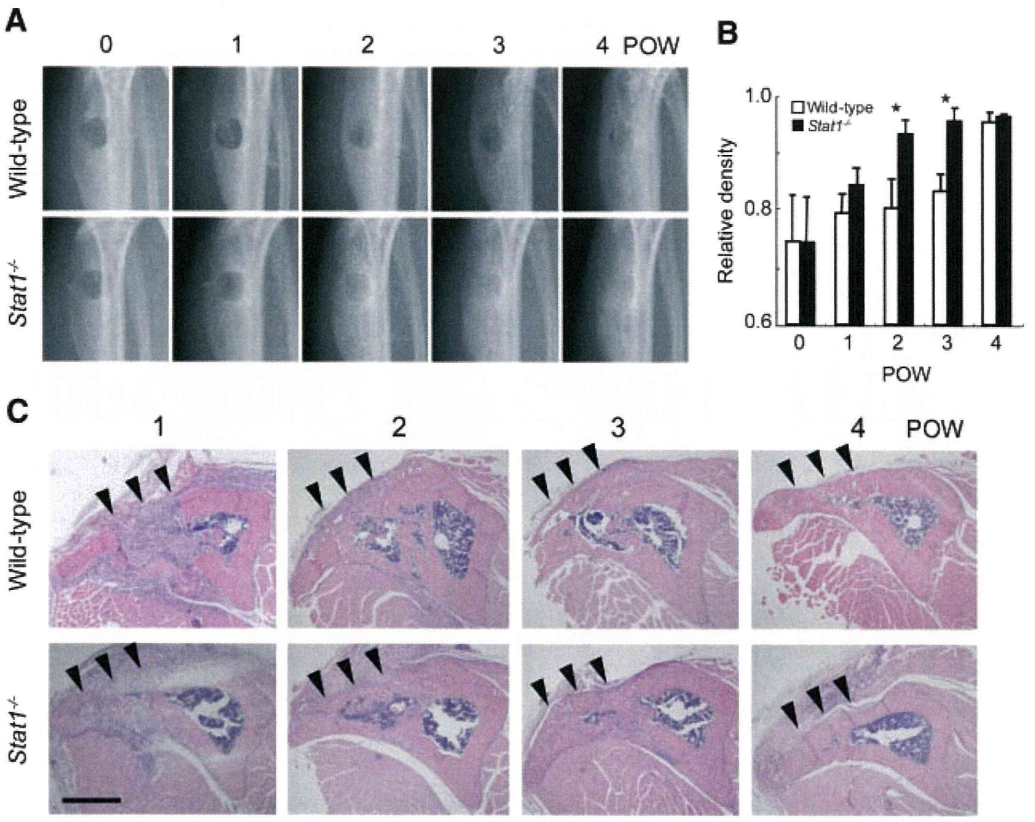

Figure 2. Membranous ossification is accelerated in *Stat1*$^{-/-}$ mice. (A) Sequential X-ray images of the tibiae with a diameter 1.0 mm cortical defect. (B) Relative X-ray intensity of the defect area in the tibiae. $n = 4$. *$p < 0.05$. (C) Histological analysis of cortical defect model. Arrowheads indicate sites of cortical defects. Scale bar, 1 mm.

in the cortical defect is highly accelerated in *Stat1*$^{-/-}$ mice compared with wild-type control when evaluated by X-rays. Histological analysis confirmed this observation (Fig. 2C). No apparent cartilage tissue was found when the sections were evaluated by alcian blue staining (data not shown). These results show that bone formation by osteoblasts (membranous ossification) is also accelerated in a STAT1-deficient environment during fracture healing.

STAT1 Negatively Regulates Osx Expression in Osteoblasts

We next sought to elucidate whether STAT1 affects the expression levels of the transcripts for Runx2 and Osx, essential transcription factors for osteoblast differentiation. POBs from wild-type and *Stat1*$^{-/-}$ newborn mice were incubated in the presence of BMP-2 and RNA was prepared at the designated time points. As shown in Figure 3A, there was no significant difference in the transcripts level of Runx2 between wild-type and *Stat1*$^{-/-}$ POBs; on the other hand, the expression levels of Osx and osteocalcin were significantly upregulated in *Stat1*$^{-/-}$ POBs, indicating that STAT1 also exerts its inhibitory effects on osteoblast differentiation via suppressing Osx transcription. To further confirm this observation, we next investigated the effects of STAT1 on the transcriptional activity of Osx by luciferase reporter assay using a reporter vector bearing *Osterix* promoter sequence.[12] Based on the previous studies showing that STAT1 binds to p65 (one of the components of NF-κB complex) and inhibits its transcriptional activity (Ref.[13–15] and data not shown), and that p65 stimulates the Osx promoter,[12] we hypothesized that downregulation of Osx transcription by STAT1 is mediated by p65. As shown in Figure 3B, although STAT1 did not show any inhibitory effect on the basal Osx transcription level in either MC3T3-E1 or COS-7 cells, p65-induced Osx transcriptional activity was effectively inhibited by STAT1 in a dose-dependent manner. To confirm that STAT1 directly inhibits p65 transcriptional activity, we also did a luciferase reporter assay using a reporter vector bearing an NF-κB response element (NF-κB-RE), and confirmed that STAT1 effectively suppresses the transcriptional activity induced by p65 (Fig. 3C). In accordance, we also found that introduction of p65 in wild-type POBs leads to an increase in the transcripts levels of Osx and osteocalcin, and that this upregulation is blocked by STAT1 (Fig. 3D). Taken together, these observations suggest that, in addition to the inhibition of the nuclear translocation of Runx2 as previously reported,[7] STAT1 also negatively regulates osteoblast differentiation by suppressing Osx transcription through inhibition of p65 activity.

STAT1 Inhibitor Accelerates Heterotopic Ossification

Based on the results of the fracture model experiments and luciferase assays that STAT1 negatively regulates osteoblast differentiation, we next asked if the ossification process in vivo could be stimulated by fludarabine, a potent inhibitor of STAT1. Fludarabine is a purine analog and used as a chemotherapeutic agent for the treatment of hematopoietic malignancies; however, it has also been shown that fludarabine reduces STAT1 phosphorylation and suppresses STAT1 protein and transcript levels.[16] We subcutaneously transplanted gelatin pellets containing BMP-2 with or without fludarabine and collected the pellets 2 weeks after the implantation. As expected, the pellets with BMP-2

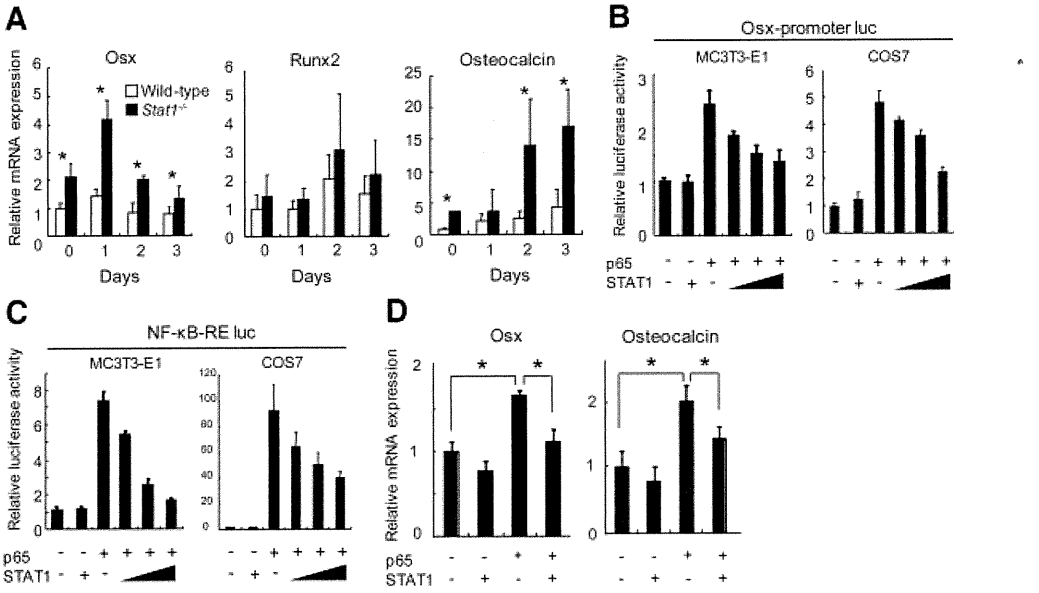

Figure 3. STAT1 suppresses Osx transcription. (A) Quantification of the transcript levels of Osx, Runx2, and osteocalcin in wild-type and *Stat1*$^{-/-}$ POBs incubated with BMP-2 as described in the Materials and Methods. Note the increased expression of Osx and osteocalcin transcripts, but not that of Runx2, in *Stat1*$^{-/-}$ POBs. (B,C) Luciferase reporter assay of Osx promoter (B) and NF-κB-RE promoter (C) in MC3T3-E1 and COS-7 cells. p65-driven promoter activity was repressed by STAT1in a dose-dependent manner. (D) Quantification of the transcript levels of Osx and osteocalcin in wild-type POBs transfected with STAT1 and/or p65 expression vector(s). *$p < 0.05$.

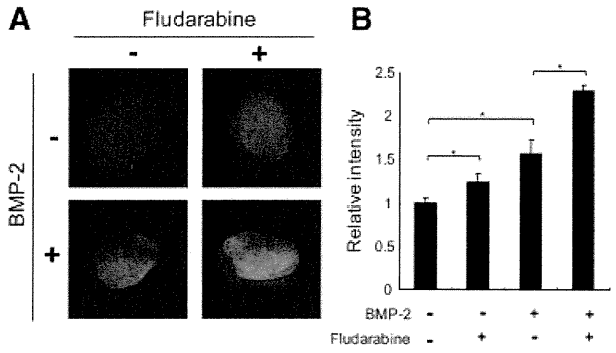

Figure 4. Inhibition of STAT1 activity by fludarabine enhances heterotopic ossification. (A) X-ray images of the subcutaneously transplanted gelatin pellets containing BMP-2 (3 μg) and/or fludarabine (10 μg). Scale bar, 1 mm. (B) Relative intensity of the X-ray images of the calcified pellets. $n = 4$. $^*p < 0.05$.

showed a marked calcification compared to the control pellets. The pellets with fludarabine alone also showed moderated upregulation in calcification; however, when fludarabine was used in combination with BMP-2, ossification of the pellets was further accelerated (Fig. 4A and B). These observations indicate that ossification process can be enhanced by suppression of STAT1 activity in vivo.

DISCUSSION

The findings in the tibial fracture model and the cortical bone defect model showed that bone formation by osteoblasts is accelerated in a STAT1-deficient environment during fracture healing. In vitro data showed STAT1 negatively regulates osteoblast differentiation by suppressing Osx transcription through inhibition of p65 activity. These results reveal a previously unknown contribution of STAT1 in the remodeling phase of the fracture healing and show that inhibition of STAT1 with fludarabine can effectively stimulate ossification in vivo. Our observations and the recent studies by others suggest that the mechanisms behind accelerated fracture healing in *Stat1*$^{-/-}$ mice is due to upregulation in bone formation (by increased Osx expression, in addition to the enhanced nuclear localization of Runx2 in osteoblasts[7]) and increased bone resorption by osteoclasts.[5,6] On the other hand, because STAT1 is also implicated in the regulation of angiogenesis and chondrogenesis;[17,18] potential contributions of other factors cannot be ruled out. Nevertheless, the results of the current study further support the notion that STAT1 as a crucial negative regulator for both osteoblast differentiation and osteoclastogenesis, and also suggest that inhibition of STAT1 activity may be beneficial for the treatment of skeletal fracture.

ACKNOWLEDGMENTS

The authors thank Shizue Tomita and Yuko Hashimoto for their excellent technical support. This study was supported by the grants of General Insurance Association of Japan.

REFERENCES

1. Burge R, Dawson-Hughes B, Solomon DH, et al. 2007. Incidence and economic burden of osteoporosis-related fractures in the United States, 2005–2025. J Bone Miner Res 22: 465–475.
2. Manolagas SC. 2000. Birth and death of bone cells: basic regulatory mechanisms and implications for the pathogenesis and treatment of osteoporosis. Endocr Rev 21:115–137.
3. Gerstenfeld LC, Cullinane DM, Barnes GL, et al. 2003. Fracture healing as a post-natal developmental process: molecular, spatial, and temporal aspects of its regulation. J Cell Biochem 88:873–884.
4. Meraz MA, White JM, Sheehan KC, et al. 1996. Targeted disruption of the Stat1 gene in mice reveals unexpected physiologic specificity in the JAK–STAT signaling pathway. Cell 84:431–442.
5. Takayanagi H, Ogasawara K, Hida S, et al. 2000. T-cell-mediated regulation of osteoclastogenesis by signalling cross-talk between RANKL and IFN-gamma. Nature 408:600–605.
6. Takayanagi H, Kim S, Matsuo K, et al. 2002. RANKL maintains bone homeostasis through c-Fos-dependent induction of interferon-beta. Nature 416:744–749.
7. Kim S, Koga T, Isobe M, et al. 2003. Stat1 functions as a cytoplasmic attenuator of Runx2 in the transcriptional program of osteoblast differentiation. Genes Dev 17:1979–1991.
8. Shimoaka T, Kamekura S, Chikuda H, et al. 2004. Impairment of bone healing by insulin receptor substrate-1 deficiency. J Biol Chem 279:15314–15322.
9. Street J, Bao M, deGuzman L, et al. 2002. Vascular endothelial growth factor stimulates bone repair by promoting angiogenesis and bone turnover. Proc Natl Acad Sci USA 99: 9656–9661.
10. Kosaki N, Takaishi H, Kamekura S, et al. 2007. Impaired bone fracture healing in matrix metalloproteinase-13 deficient mice. Biochem Biophys Res Commun 354:846–851.
11. Matsubara T, Kida K, Yamaguchi A, et al. 2008. BMP2 regulates Osterix through Msx2 and Runx2 during osteoblast differentiation. J Biol Chem 283:29119–29125.
12. Lu X, Gilbert L, He X, et al. 2006. Transcriptional regulation of the osterix (Osx, Sp7) promoter by tumor necrosis factor identifies disparate effects of mitogen-activated protein kinase and NF kappa B pathways. J Biol Chem 281:6297–6306.
13. Suk K, Kim YH, Chang I, et al. 2001. IFNalpha sensitizes ME-180 human cervical cancer cells to TNFalpha-induced apoptosis by inhibiting cytoprotective NF-kappaB activation. FEBS Lett 495:66–70.
14. Hayashi T, Ishida Y, Kimura A, et al. 2007. IFN-gamma protects cerulein-induced acute pancreatitis by repressing NF-kappa B activation. J Immunol 178:7385–7394.
15. Ganster RW, Guo Z, Shao L, Geller DA. 2005. Differential effects of TNF-alpha and IFN-gamma on gene transcription mediated by NF-kappaB-Stat1 interactions. J. Interferon Cytokine Res 25:707–719.
16. Plosker GL, Figgitt DP. 2003. Oral fludarabine. Drugs 63: 2317–2323.
17. Battle TE, Lynch RA, Frank DA. 2006. Signal transducer and activator of transcription 1 activation in endothelial cells is a negative regulator of angiogenesis. Cancer Res 66:3649–3657.
18. Sahni M, Raz R, Coffin JD, et al. 2001. STAT1 mediates the increased apoptosis and reduced chondrocyte proliferation in mice overexpressing FGF2. Development 128:2119–2129.

Bone 47 (2010) 756–765

Contents lists available at ScienceDirect

Bone

journal homepage: www.elsevier.com/locate/bone

Epinephrine accelerates osteoblastic differentiation by enhancing bone morphogenetic protein signaling through a cAMP/protein kinase A signaling pathway

Takuya Uemura *, Yoichi Ohta, Yoshihiro Nakao, Tomoya Manaka, Hiroaki Nakamura, Kunio Takaoka

Department of Orthopaedic Surgery, Osaka City University Graduate School of Medicine, Osaka, Japan

ARTICLE INFO

Article history:
Received 20 February 2010
Revised 7 July 2010
Accepted 7 July 2010
Available online 13 July 2010

Edited by: R. Baron

Keywords:
Bone morphogenetic protein
epinephrine
catecholamine
3', 5'-cyclic adenosine monophosphate
osteoblastic differentiation
β2-adrenergic receptor

ABSTRACT

Topical effects of a catecholamine on bone morphogenetic protein (BMP)-induced ectopic bone formation were investigated in both *in vivo* and *in vitro* experimental systems. Epinephrine enhanced bone induction by BMP-2. Thus, the mass of ossicles ectopically induced by BMP-2 (5 μg) was increased by the addition of a low dose (10, 20, 40, or 80 μg) of epinephrine into a biodegradable BMP-2 carrier, in a dose-dependent manner. To investigate the mechanism by which epinephrine enhances BMP activity, *in vitro* experiments were carried out using osteogenic cells. The expression level of alkaline phosphatase (ALP) in cells, a marker of osteoblastic differentiation, was consistently elevated by BMP-2 (50 ng/ml) and was further elevated by the addition of epinephrine (10^{-8} M). The epinephrine-enhanced ALP elevation was specifically abolished by an antagonist to β2-adrenergic receptors (Butoxamine) and by a protein kinase A inhibitor (H89). Furthermore, BMP-induced mRNA expression of ALP and osteocalcin (marker proteins of osteoblastic differentiation) and of Osterix (a transcription factor essential for terminal differentiation to osteoblasts) in ST2 cells was significantly enhanced by the addition of epinephrine (10^{-8} M). In luciferase expression assays using the promoter sequence of the Id1 gene (an immediate early response gene to BMP), luciferase activity was elevated by BMP-2 treatment (50 ng/ml) and this activity was further enhanced by the addition of epinephrine (10^{-8} M). Epinephrine-enhanced luciferase activity was abolished by mutation of the cAMP-response element (CRE) sequence in the Id1 promoter, indicating that CRE-binding transcription proteins induced by epinephrine addition may act as enhancers of Smad-mediated BMP signaling.

Introduction

Recent reports indicate the involvement of catecholamines in the regulation of bone metabolism through activation of Gs-coupled adrenergic receptors [1–5], located on both osteoblasts and osteoclasts [6–9], and through elevation of intracellular cyclic adenosine 3′, 5′-monophosphate (cAMP) levels [10–14].

Our previous study indicated that intracellular cAMP accumulation consistently enhances bone morphogenetic protein (BMP)-mediated osteoblastic differentiation of mesenchymal cells and that this effect is regulated by enhancement of Smad-mediated transcriptional activity through the protein kinase A (PKA)/cAMP-response element-binding protein (CREB) signaling pathway [15–20]. In this context, we hypothesized that catecholamines might also have a potential role in enhancement of BMP-induced osteoblastic differentiation and subsequent bone formation. The present study was designed to clarify the effects of epinephrine on BMP-induced ectopic bone formation in an *in vivo* experimental system and to gain an insight into cross talk between intracellular BMP-induced signaling and catecholamine-signaling pathways using an *in vitro* system.

Materials and methods

Animal care and protocols for in vivo experiments

Male ICR mice (5 weeks old) were purchased from Japan SLC, Inc. (Hamamatsu, Japan) and were housed in an air-conditioned room with free access to food and water. After acclimation for 1 week, experiments were carried out in strict accordance with the Institutional Guidelines for the Care and Use of Laboratory Animals of Osaka City University.

* Corresponding author. Department of Orthopaedic Surgery, Osaka City University Graduate School of Medicine 1-4-3, Asahi-machi, Abeno-ku, Osaka 545-8585, Japan. Fax: +81 6 6646 6260.
E-mail address: t-uemura@med.osaka-cu.ac.jp (T. Uemura).

8756-3282/$ – see front matter © 2010 Elsevier Inc. All rights reserved.
doi:10.1016/j.bone.2010.07.008

Preparation of pellet implants for ectopic bone induction by BMP-2

A biodegradable polymer, poly-$_{D,L}$-lactic acid-*p*-dioxanone-polyethylene glycol (PLA-DX-PEG) block copolymer (MW: 9800, PLA/DX/PEG molar ratio: PLA/DX/PEG = 43/14/43) (Taki Chemicals Co., Kakogawa, Japan) was used for local delivery of BMP-2. The physicochemical characteristics and the efficacy of this biodegradable polymer as a carrier material for BMP have been previously reported [15,16,21–24].

To prepare BMP-2-containing pellet implants, 30 mg of the PLA-DX-PEG polymer was mixed with an aliquot of either the BMP-2 (5 μg/pellet) solution alone or with various doses of epinephrine (10, 20, 40, 80 or 160 μg/pellet) with or without BMP-2 (5 μg/pellet) and were then fashioned into discs for implantation. Various doses of fenoterol, a β2-adrenergic receptor selective agonist, (10, 20, 40 or 80 μg/pellet) were also mixed with 30 mg of the PLA-DX-PEG polymer, with or without BMP-2 (5 μg/pellet), using the same methods. All procedures were carried out under sterile conditions. The pellet implants were stored at −80 °C in a freezer until surgical implantation.

Protocol of in vivo experiment

The mice were anesthetized by diethyl-ether gas inhalation and the PLA-DX-PEG polymer discs, prepared as described above, were surgically implanted into the left dorsal muscle pouches (one pellet per animal) of the mice. Three weeks after surgery, the mice were sacrificed. The ossicles induced at the sites of implantation were explored and were then harvested and processed for radiological examination.

Radiological and histological analyses

All harvested bony tissues were radiographed using a soft X-ray apparatus (Soft Co., Ltd., Tokyo, Japan). The bone mineral content (BMC) in each ossicle was measured by dual-energy X-ray absorptiometry (DXA) using a bone mineral analyzer (DCS-600EX, Aloka Co., Tokyo, Japan). The ossicles were then fixed in neutralized 10% formalin and embedded in methyl methacrylate (MMA, Wako, Japan). Ossicle sections (7 μm thick) were cut and stained with hematoxylin–eosin.

Reagents for in vitro experiments

Recombinant human BMP-2 (BMP-2) was produced and kindly provided by Osteopharma, Inc. (Osaka, Japan) [24]. Epinephrine and fenoterol, were purchased from Sigma Chemical Co. (St. Louis, MO, USA). Epinephrine was dissolved in 0.5 M hydrochloric acid for storage [25]. The following specific antagonists were used: an antagonist to α1-adrenergic receptor subtypes Prazosin (Sigma Chemical Co.), an antagonist to β2-adrenergic receptor subtypes Butoxamine (Sigma Chemical Co.), the PKA inhibitor H89 (Sigma Chemical Co.), the PKC inhibitor Gö6976 (Calbiochem Co.), the p38 mitogen-activated protein kinase (MAPK) inhibitor SB203580 (Sigma Chemical Co.), the MEK/ERK-kinase inhibitor PD98059 (Calbiochem Co.) and the c-Jun NH2-terminal kinase (JNK) inhibitor SP600125 (Calbiochem Co.).

Cell cultures

BMP-2-responsive pluripotent murine bone marrow-derived stromal cells (ST2) and pluripotent myoblastic cells (C2C12) were obtained from the Riken Cell Bank (Ibaragi, Japan). Primary calvarial osteoblasts were isolated from a newborn ICR mouse as described previously [26]. Cells were cultured in α-minimal essential medium (α-MEM; Sigma Chemical Co.) supplemented with 10% heat-inactivated fetal bovine serum (FBS; Gibco, Grand Island, NY, USA) or 2.5% FBS and antibiotics/antimycotic (100 U/ml penicillin; 100 μg/ml streptomycin; and 0.25 μg/ml amphotericin B; Sigma Chemical Co.) at 37 °C in 5% CO_2-humidified air. Upon reaching confluence, the cells were used in the following experiments.

Detection of adrenergic receptor subtypes

Total RNA (3 μg) was isolated from the respective cell lines and primary osteoblasts using NucleoSpin RNA II (Macherey-Nagel, Duren, Germany) according to the manufacturer's instructions and was reverse-transcribed into first-strand cDNA using an oligo-dT primer and Superscript II reverse transcriptase (Invitrogen, Carlsbad, CA, USA). PCR amplification was performed using gene-specific PCR primers and rTaq (Takara Bio, Otsu, Japan). A thermal cycle reaction was carried out at 95 °C for 4 min, followed by 35 cycles at 94 °C for 30 s, 60 °C for 30 s, 72 °C for 1 min, and 72 °C for 5 min. The sequences of the PCR primers used were as follows; α1b-adrenergic receptor (forward, 5'-GTGACATCTGGGCAGCGGTTGATG-3'; reverse, 5'-ATGACCGCCAGTGGGATGTAGAAG-3'; amplicon size 304 bp) [9], α1d-adrenergic receptor (forward, 5'-CGCTGTGGTGGGAACCGGCAG-3'; reverse, 5'-ACAGCTGCACTCAGTAGCAGGTCA-3'; amplicon size 282 bp) [9], and β2-adrenergic receptor (forward, 5'-GGTTATCGTCCTGGCCATCGTGTTTG-3'; reverse, 5'-TGGTTCGTGAAGTCACAGCAAGTCTC-3'; amplicon size 468 bp) [27]. The PCR products were separated by electrophoresis on a 1% agarose gel and were visualized by staining with ethidium bromide.

Assay of intracellular cAMP

When cultured cells in 12-well plates ($n = 3$) reached confluence, the medium was replaced with fresh medium without FBS and the cells were pre-incubated for 1 h. Epinephrine (10^{-8} M) was then added once to the culture (single treatment), or epinephrine (10^{-9} M) was added 10 times at 3-min time intervals (cyclic treatments) resulting in a final cumulative concentration of epinephrine of 10^{-8} M. After further incubation for 1 min, 2.5 min, 5 min, 10 min, 15 min, 30 min, 1 h, 2 h and 3 h, the medium was removed and the cAMP level in the cultured cells was determined using a cAMP enzyme immunoassay system (GE Healthcare, Piscataway, NJ, USA) in accordance with the manufacturer's instructions. All experiments were performed independently in triplicate.

Assay of alkaline phosphatase (ALP) activity

Cells were seeded at a density of 2×10^4 cells per well in 24-well plates ($n = 4$). When the cells reached confluence, the medium was replaced with fresh treatment medium containing 2.5% FBS and BMP-2 (50 ng/ml). Cells (ST2, C2C12 or primary osteoblasts) were additionally stimulated by epinephrine using cyclic treatments (with a final cumulative concentration of epinephrine of 10^{-8} M) as described above, and were then cultured for an additional 3, 6 or 3 days, respectively. ST2 cells were also stimulated by cyclic fenoterol treatments (10 cycles of 10^{-8} M at 3-min time intervals, resulting in a final cumulative concentration of 10^{-7} M) with or without BMP-2 (50 ng/ml) and were then cultured for an additional 3 days. ALP levels were measured using *p*-nitrophenylphosphate as the ALP substrate and the obtained data were normalized to cellular protein levels (Bio-Rad Laboratories, Hercules, CA, USA). All experiments were performed independently in triplicate.

Effects of protein kinase inhibitors

To identify the adrenergic receptor subtype that mediates epinephrine signaling in order to modulate BMP signaling, the effect of antagonists specific to the α1-adrenergic receptor subtype (Prazosin; 10^{-7} M) or the β2-adrenergic receptor subtype

(Butoxamine; 10^{-6} M) on epinephrine activity was assayed. To identify protein kinases involved in the intracellular signaling induced by epinephrine, the effect of specific inhibitors of PKA (H89; 2 μM), PKC (Gö6976; 10^{-8} M), the p38 MAPK (SB203580; 10^{-8} M), MEK/ERK-kinase (PD98059; 10^{-8} M) or JNK (SP600125; 10^{-8} M) on epinephrine enhancement of BMP-induced ALP activity was assayed. ST2 cells were pre-treated with medium containing 2.5% FBS and the respective inhibitor for 2 h. BMP-2 (50 ng/ml) and/or epinephrine (10 cycles of 10^{-9} M) were then added to the media containing the inhibitors, and incubation was continued in this inhibitor-containing media for another 3 days. The mean level of ALP activity in the cells was determined from triplicate samples.

Quantitative real-time reverse transcription polymerase chain reaction

The medium of confluent ST2 cells in 6-well plates ($n=3$) was replaced with fresh medium containing 2.5% FBS and BMP-2 (50 ng/ml), and the cells were treated with or without epinephrine (10 cycles of 10^{-9} M). At each time point, total RNA was isolated from the cells using NucleoSpin RNA II (Macherey-Nagel, Duren, Germany) according to the manufacturer's instructions. Total RNA (5 μg) was reverse-transcribed into first-strand cDNA with an oligo-dT primer using Superscript II reverse transcriptase (Invitrogen). Real-time reverse transcription polymerase chain reaction (RT-PCR) was performed according to the manufacturer's instructions (Applied Biosystems, Foster City, CA, USA) using an iCycler apparatus (Bio-Rad Laboratories) and iCycler Optical System Interface software (version 3.0; Bio-Rad Laboratories). TaqMan fluorogenic probes for Osterix, ALP, osteocalcin and GAPDH (an internal control) were purchased from Applied Biosystems. Real-time RT-PCR was performed using Absolute QPCR low rox Mixs (Applied Biosystems). To correct variability in RNA recovery and efficiency of reverse transcription, GAPDH cDNA was amplified and quantified for each cDNA preparation. Steps of normalization and calculation were

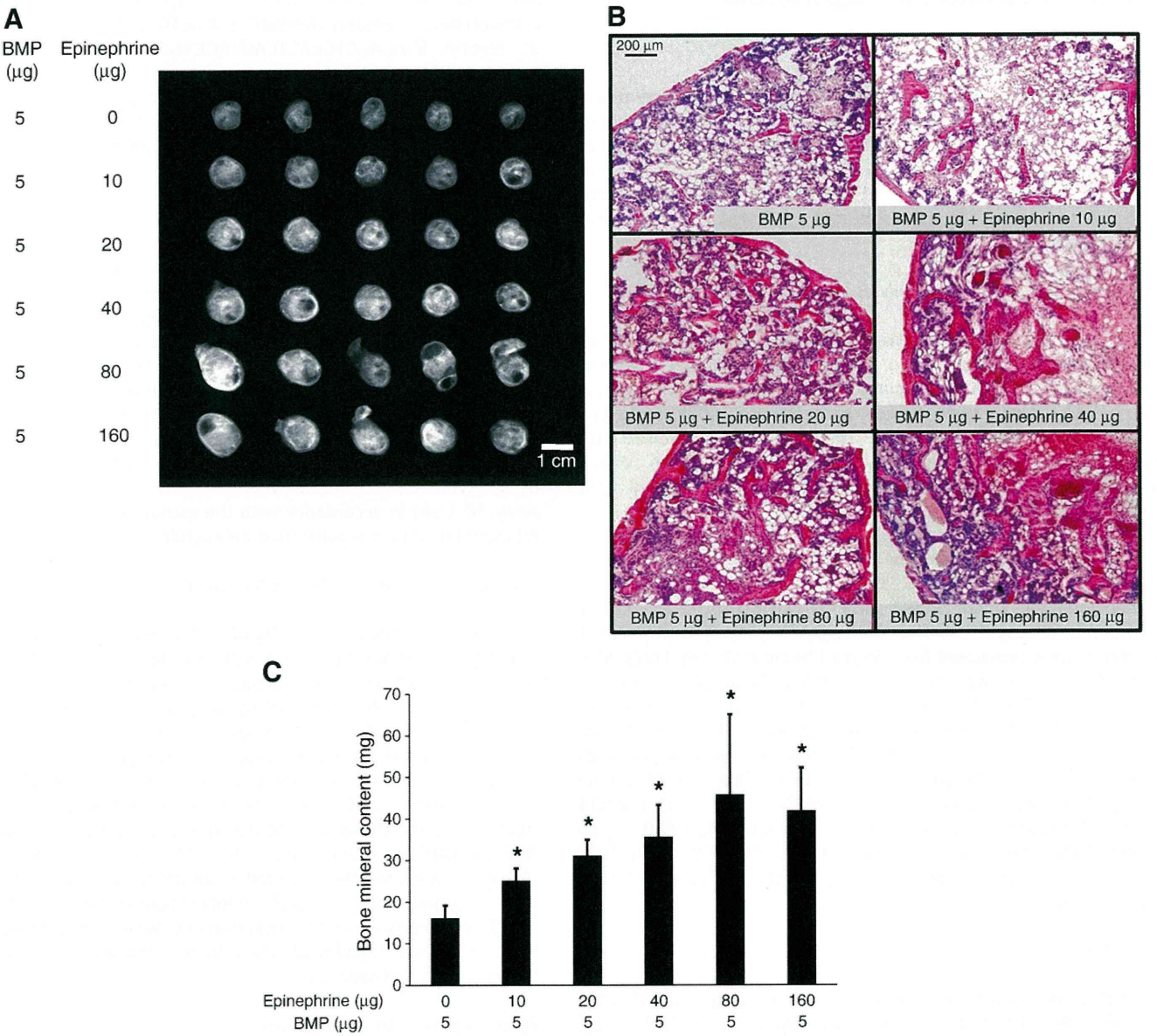

Fig. 1. Effect of epinephrine on BMP-2-induced ossicles. Mice were implanted with implants containing 5 μg BMP-2 and the indicated concentration of epinephrine. Three weeks after implantation newly formed ossicles were examined (A) by soft X-ray photography, (B) by hematoxylin and eosin staining and (C) for bone mineral content. In (A) both the radio-opaque areas and the radiological densities of the ossicles were larger in the groups stimulated by epinephrine than in the BMP-2 alone group (control). In (B), epinephrine addition induced visible increases in the number and thickness of bony trabeculae compared to those in the ossicles of the control group. In (C), the BMC of the ossicles peaked at 80 μg of added epinephrine. Bars and lines represent mean ± SD for 5 samples. *$p<0.05$.

performed as described by Pfaffl [28]. All experiments were performed independently in triplicate.

Id1 gene promoter-linked luciferase gene expression

A luciferase reporter plasmid driven by the Id1 promoter (Id985WT-luc) was kindly provided by Dr. Katagiri (Saitama Medical School, Saitama, Japan) [29]. Id1 is known to be an early response gene to BMP-2, to contain both a BMP-responsive element (BRE) and a cAMP-response element (CRE) [19], and to commit young mesenchymal cells to differentiate into osteoblasts. To investigate the effects of epinephrine on BMP-induced transcriptional activity in ST2 cells, we used wild-type luciferase reporter plasmids and a CRE-mutated Id1 promoter as described previously [19,20].

For the reporter assay, ST2 cells were plated at a density of 4×10^3 cells per well in 96-well plates ($n=4$) and were then cultured until almost confluent before transfection of the luciferase gene. Cells were transfected with reporter plasmid constructs containing a BRE and a wild-type or a mutated CRE, using Lipofectamine 2000 according to the manufacturer's instructions (Invitrogen). At 5 h after transfection, the medium was replaced with fresh medium, and the cells were then treated with BMP-2 (50 ng/ml), and/or epinephrine (10 cycles of 10^{-9} M) for a further 24 h. Cells were then harvested, and luciferase activity in the cell extracts was determined using a Dual-Glo Luciferase assay system (Promega, Madison, WI, USA). All experiments were performed independently in triplicate.

Statistical analysis

Data are expressed as the mean ± standard deviation (SD) for each group. Differences between treatment groups were analyzed using Fisher's Protected Least Significant Difference (PLSD) test. Values of $p<0.05$ were considered statistically significant.

Results

Effect of epinephrine on ectopic bone formation by BMP-2

The ectopic ossicles that were induced by PLA-DX-PEG polymer discs containing BMP-2 (5 μg) without or with epinephrine (10, 20, 40, 80 and 160 μg) are shown in Fig. 1. No evidence of ossicle formation was found in groups implanted with polymer discs with epinephrine alone without BMP-2 (data not shown). Ossicles induced by BMP-2 in conjunction with epinephrine were of a significantly larger size on soft X-ray radiograms (Fig. 1A) and showed significantly higher bone mineral content (BMC) on DXA, than those of ossicles induced by BMP-2 alone without epinephrine (control) (Fig. 1C). The mean BMC value of ossicles in the epinephrine (80 μg) + BMP-2 (5 μg)-treated group was approximately 3 times higher than that of the BMP-2 group without epinephrine. Histological sections of all ossicles showed normal bone characteristics with trabeculae and bone marrow (Fig. 1B). In the BMP-2 + epinephrine-treated groups, the number and thickness of bony trabeculae were visibly increased compared to the ossicles of the control group (BMP-2 alone).

Elevation of intracellular cAMP levels by epinephrine

We next determined the best conditions for induction of intracellular cAMP by epinephrine. Elevation of intracellular cAMP concentration was consistently noted in all cultured cells following epinephrine treatment. The profile of cAMP elevation by epinephrine stimulation was similar in the ST2, C2C12 and primary osteoblastic cells (data not shown). In ST2 cells, the epinephrine-elevated cAMP level was maintained for a longer time if epinephrine was added by 10 cyclic additions at a low dose (10^{-9} M), rather than by addition

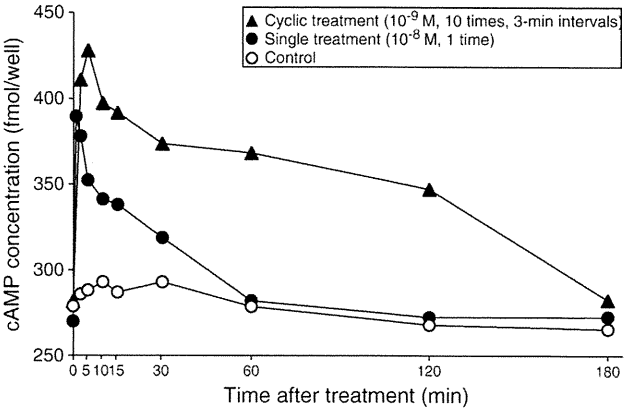

Fig. 2. Elevation of Intracellular cAMP levels by epinephrine. Cultured ST2 cells were stimulated with 10^{-8} M epinephrine, which was administered as a single high dose (10^{-8} M) or administered 10 times at 3-min intervals using a low dose (10^{-9} M) of epinephrine each time. The intracellular cAMP level was then measured using an ELISA. Intracellular cAMP remained elevated for a longer time following cyclic stimulation with low doses of epinephrine.

using a single high dose (10^{-8} M) (Fig. 2). Based on these results, epinephrine stimulation was carried out throughout the study by cyclic additions of the low dose (10 cycles of 10^{-9} M at 3-min time intervals, resulting in a final cumulative concentration of 10^{-8} M).

Expression of adrenergic receptor subtypes in osteogenic cells

Prior to analysis of the adrenergic receptors through which epinephrine might modulate BMP functions, we first confirmed the previously reported expression [7,14,30,31] of α1b-, α1d- and β2-adrenergic receptor subtypes genes in ST2, C2C12 and primary osteoblast cells by RT-PCR (Fig. 3). Of the two receptor subtypes, the β2-adrenergic receptor but not the α1d-receptor, is known to mediate epinephrine-induced intracellular cAMP accumulation [12,32–34]. To examine the potential involvement of the β2-adrenergic receptor in the anabolic action of epinephrine in BMP-2-induced bone formation, we tested the effect of addition of fenoterol, a β2-adrenergic receptor specific agonist, in place of epinephrine, in both the *in vivo* and *in vitro* systems, and analyzed its effect on BMP-2-induced ectopic bone formation. The effect of fenoterol was equivalent to that of epinephrine (Fig. 4), suggesting that the β2-

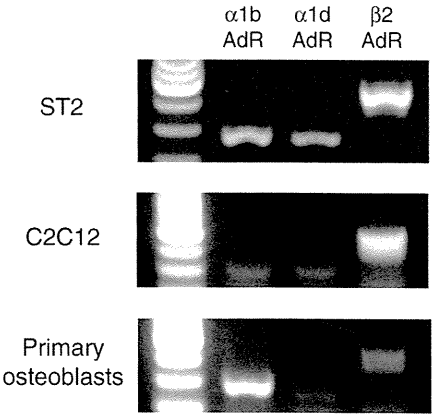

Fig. 3. The mRNA expression of adrenergic receptor subtypes in osteogenic cells. Total RNA, extracted from ST2 and C2C12 cells and from primary calvarial osteoblasts, was analyzed by RT-PCR using primers specific for each adrenergic receptor subtype. PCR products were analyzed by agarose gel electrophoresis. Molecular weight markers are at left. The mRNA expression of α1b-, α1d- and β2-adrenergic receptor subtypes was detectable in all of the cells tested. α1bAdR: α1b-adrenergic receptor, α1dAdR: α1d-adrenergic receptor, β2AdR: β2-adrenergic receptor.

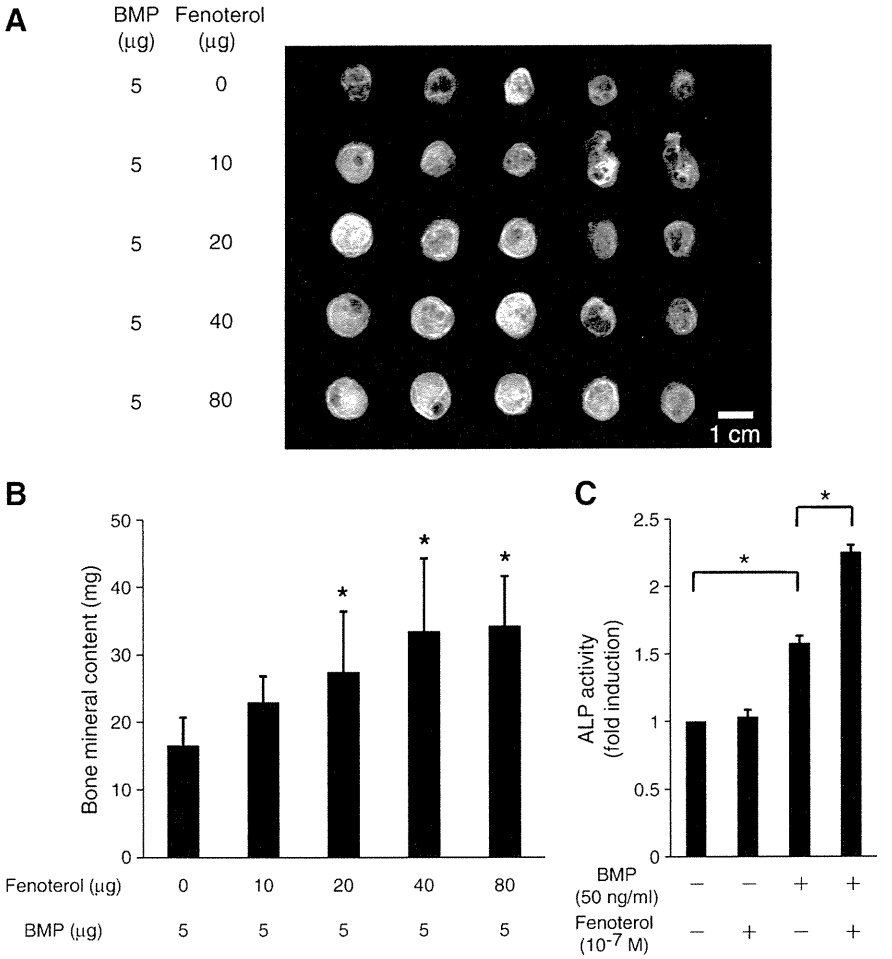

Fig. 4. Effect of fenoterol on BMP-2-induced ossicles and on ALP induction by BMP-2 in ST2 cells. The ectopic ossicles in mice that were induced by PLA-DX-PEG polymer discs containing BMP-2 (5 μg) without or with fenoterol (10, 20, 40 and 80 μg) are shown. Ossicles induced by BMP-2 in conjunction with fenoterol were of a significantly larger size on soft X-ray radiograms in (A) and showed significantly higher bone mineral content (BMC) on DXA in (B), than those of ossicles induced by BMP-2 alone without fenoterol (control). ST2 cells were stimulated by cyclic fenoterol treatment (10 cycles of 10^{-8} M at 3-min time intervals, resulting in a final cumulative concentration of 10^{-7} M) with or without BMP-2 (50 ng/ml) and were then cultured for an additional 3 days. (C) The ALP levels of ST2 cells were elevated in response to BMP-2 (50 ng/ml), and the BMP-2-induced ALP levels were further enhanced by the addition of fenoterol. ALP activity was normalized to that of the control group which was assigned a value of 1. The bars and lines represent the mean ± SD of 4 wells. BMP: BMP-2 (50 ng/ml), fenoterol (10^{-7} M): fenoterol (10^{-8} M) was added 10 times at 3-min intervals, $^{*}p<0.05$.

adrenergic receptor is involved in mediation of the epinephrine-induced enhancement of BMP actions.

ALP induction by BMP-2 and/or epinephrine

The ALP levels of ST2, C2C12 and osteoblast cells were elevated in response to BMP-2 (50 ng/ml), and these BMP-2-induced ALP levels were further enhanced by the addition of epinephrine (Fig. 5). To investigate the intracellular signaling pathway by which epinephrine enhances BMP-2 signaling, we first assayed the effects of antagonists of adrenergic receptor subtypes in ST2 cells. A specific antagonist to β2-adrenergic receptor subtypes (Butoxamine) abolished epinephrine enhancement of BMP-2 signaling, whereas a specific antagonist to α1-adrenergic receptor subtypes (Prazosin) did not inhibit epinephrine-induced enhancement of BMP-2-induced ALP activity (Fig. 6A). To identify protein kinases involved in the intracellular signaling induced by epinephrine, the effect of specific inhibitors of PKA (H89), PKC (Gö6976), the p38 MAPK (SB203580), MEK/ERK-kinase (PD98059) and JNK (SP600125) on epinephrine enhancement of BMP-induction of ALP was assayed. H89 significantly abolished this epinephrine-induced effect (Fig. 6B). However, neither Gö6976 (Fig. 5B), nor SB203580, PD98059 or SP600125 (Fig. 6C) inhibited this epinephrine activity. Based on these results, it was concluded that epinephrine enhanced BMP-induced-osteoblastic differentiation, mainly through the PKA signaling pathway, via β2-adrenergic receptors.

Enhancement of BMP-2-induced mRNA expression of ALP, osteocalcin and Osterix by epinephrine

Induction of osteoblastic differentiation by BMP-2 involved enhancement of the mRNA expression of both the osteoblastic differentiation markers ALP and osteocalcin, as well as that of Osterix, which is a key transcriptional regulator for osteoblastic differentiation. In ST2 cells, epinephrine addition also enhanced BMP-2 upregulation of these mRNAs as assayed on days 3, 6 and 3, respectively, following epinephrine addition (Fig. 7A–C). These results indicate that epinephrine potentially enhanced BMP-2-induced mRNA expression of osteoblastic differentiation markers.

Id1 promoter-driven luciferase expression by BMP-2 and/or epinephrine

Upregulation of osteoblastic differentiation-specific cellular mRNA by BMP-2 suggested that BMP-2 may act by modulating transcriptional events. Indeed we have shown that epinephrine modulates

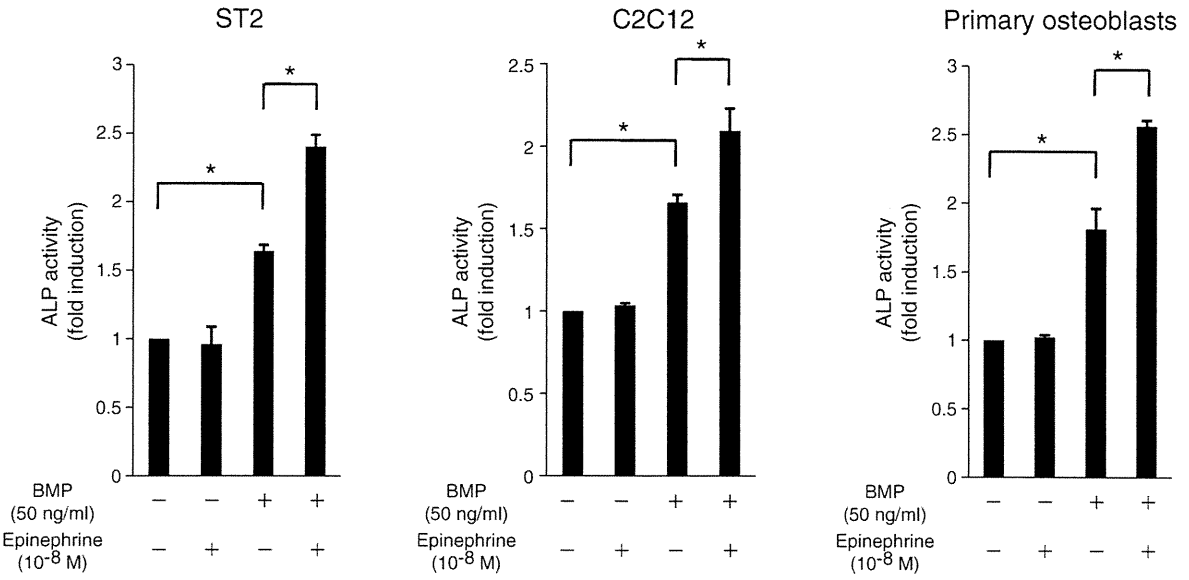

Fig. 5. Effect of epinephrine on ALP induction by BMP-2 in osteogenic cells. ST2 cells, C2C12 cells, and primary calvarial osteoblasts, were treated with BMP-2 (50 ng/ml) and/or epinephrine (10^{-8} M), or with buffer control, and ALP activity was assayed in ST2 cells and primary osteoblasts after 3 days and in C2C12 cells after 6 days. At these times, BMP-2 activated ALP in all cells and this activity was further enhanced by epinephrine. ALP activity was normalized to that of the control group which was assigned a value of 1. The bars and lines represent the mean ± SD of 4 wells. BMP: BMP-2 (50 ng/ml), Epinephrine (10^{-8} M): epinephrine (10^{-9} M) was added 10 times at 3-min intervals, $^{*}p<0.05$.

Smad-mediated transcription resulting in the generation of specific mRNAs. To determine if epinephrine enhances BMP-2-modulated transcription by upregulation of cAMP and subsequent CRE activation by binding of activated transcription factor(s), we assayed the effect of epinephrine addition on the activity of a luciferase reporter with an Id1 promoter that contains both BRE and CRE. Elevation of luciferase activity in ST2 cells in response to BMP-2 treatment was further up-regulated by the addition of epinephrine (Fig. 8A). This epinephrine-induced upregulation was not observed in cells transfected with a luciferase gene in which the CRE sequence in the Id1 promoter was mutated (Fig. 8B), indicating that epinephrine accelerates BMP signaling through CRE-mediated transcriptional regulation.

Discussion

A catabolic action of catecholamines in bone metabolism has been suggested based on *in vivo* experimental systems [1–5]. In contrast, the present study showed an anabolic effect of epinephrine on BMP-2-induced ectopic new bone formation under *in vivo* conditions that manifested as an increase in size and in the BMC of BMP-2-induced ectopic ossicles. One possible explanation of the discrepancy between these effects of epinephrine on bone metabolism under *in vivo* conditions may be due to the concentrations and/or method of delivery of epinephrine in the different studies. Enhanced osteoclastogenesis, resulting in systemic bone loss, is known to occur during physiological systemic bone remodeling, which is regulated by various endocrine systems. Thus, repeated systemic administration of significant doses of epinephrine may have a catabolic effect on bone metabolism whereas continuous local release of lower doses of epinephrine from the biodegradable carrier may result in anabolic effects. A second possible explanation of this discrepancy may be that the anabolic effect of epinephrine on bone formation is confined to BMP-induced ectopic bone, which is exposed to the low dose of epinephrine that is continuously released from the pellet implants concomitant with BMP-2. This extremely low dose epinephrine is unlikely to strongly modulate systemic bone metabolism. Further study of the effects of continuously released, low dose epinephrine from implants on systemic bone metabolism is required to clarify this matter.

We also investigated the mechanism by which epinephrine enhances BMP-2 action using an *in vitro* system. As expected from previous classical reports, epinephrine addition to osteogenic cells instantly elevated the intra-cellular cAMP level [10–14]. This reaction of osteogenic cells to epinephrine appears to be mediated through β-adrenergic receptors based on the adrenergic receptor expression profile of the osteogenic cells and on the inhibition of this effect of epinephrine by a specific β-adrenergic receptor antagonist [10,12,33]. The expression profiles of adrenergic receptors that were observed by RT-PCR in the osteogenic cells, were in accordance with those of previous reports [7,14,30,31]. Moreover, the epinephrine-induced up-regulation of cAMP via β2-adrenergic receptors is consistent with the known activity of these receptors, which activate adenylylcyclase via G protein [35] to produce cAMP.

In order to maintain an elevated level of cAMP in the cells, cyclic (ten times) stimulation using a low dose (10^{-9} M) of epinephrine at each cycle, was a more effective way to administer epinephrine than using a single equivalent dose (10^{-8} M). Although the mechanism of this phenomenon remains unclear, as well as the our results (Fig. 2) are consistent with a previous report previous report that high levels of intracellular cAMP were maintained with cyclic stimulation of PTH [20]. We speculate that mechanisms that regulate intracellular cAMP-degrading phosphodiesterases may be involved in generation of the different intracellular cAMP retention profiles.

The level of enzymatic activity of ALP, a marker of osteoblastic differentiation for undifferentiated mesenchymal cells, was utilized as an index of BMP activity in the experiments on the effects of epinephrine on BMP-2-induced osteoblastic differentiation. Epinephrine enhanced BMP-induced ALP levels in all of the cells tested: ST2, C2C12 and primary osteoblastic cells (Fig. 5). Therefore, ST2 cells were used as representative cells for the rest of the study.

Although PKA and/or PKC have been reported to be activated by elevated levels of cAMP, epinephrine enhancement of BMP action was inhibited exclusively by a PKA specific inhibitor (H89) and not by a PKC inhibitor (Fig. 6). This finding that PKA plays a more important role than PKC in modulation of BMP-2 signaling is similar to the result

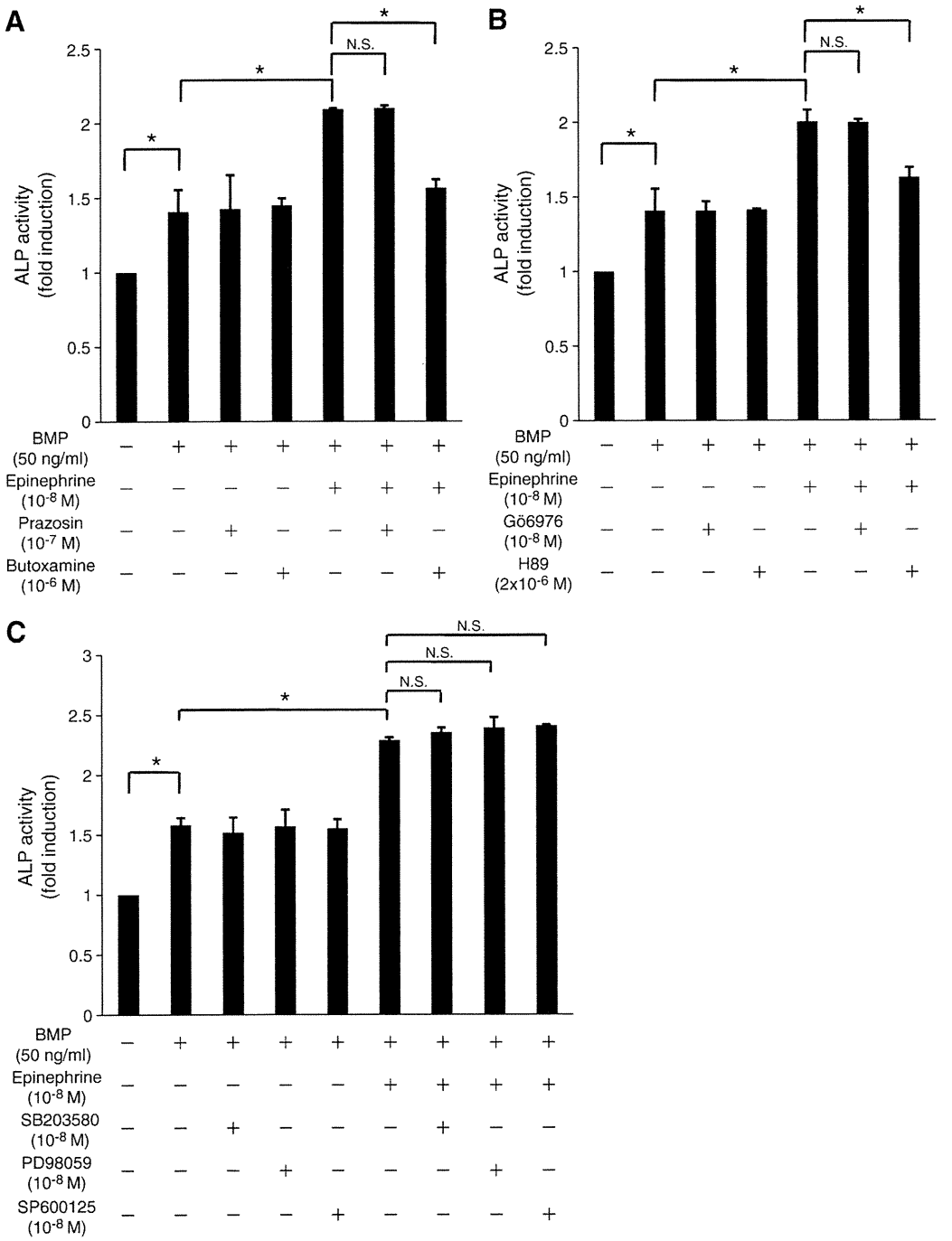

Fig. 6. Effect of adrenergic receptor subtype antagonists and protein kinase inhibitors on epinephrine-enhancement of BMP-2-induced ALP activity. ST2 cells were pre-incubated for 2 h without or with (A) a specific antagonist to α1-adrenergic (Prazosin; 10^{-7} M), or to β2-adrenergic (Butoxamine; 10^{-6} M) receptor subtypes, (B) a specific inhibitor of PKC (Gö6976; 10^{-8} M) or PKA (H89; 2 μM) or (C) a specific inhibitor of the p38 MAPK (SB203580; 10^{-8} M), MEK/ERK-kinase (PD98059; 10^{-8} M), or JNK (SP600125; 10^{-8} M). The cells were then incubated in the continued presence of the antagonists or inhibitors for an additional 3 days, with BMP-2 (50 ng/ml) in the presence or absence of epinephrine, or with buffer control. The epinephrine enhancement of BMP-induced ALP was abolished only by the specific antagonist to the β2-adrenergic receptor subtype and the specific inhibitor of PKA (H89) but not by the other inhibitors tested. The ALP value of the control group was assigned a value of 1. The bars and lines represent the mean ± SD of 4 wells. BMP: BMP-2 (50 ng/ml), Epinephrine (10^{-8} M): epinephrine (10^{-9} M) added 10 times at 3-min intervals, N.S.: not significant, $^{*}p<0.05$.

of our previous study in which PKA played a critical role in PTH (teriparatide) enhancement of BMP-2 activity [20]. It has been reported that stimulation of β2-adrenergic receptor activates the p38 MAPK [36,37], MEK/ERK-kinase [38,39] and JNK [40,41] in addition to the cAMP/PKA signaling pathway. Cross-talk between the cAMP/PKA pathway and the p38 MAPK pathway in β2-adrenergic receptor signaling has also been demonstrated previously [36]. However, in the present study, enhancement of BMP activity by epinephrine was not abolished by inhibitors of p38 MAPK, MEK/ERK-kinase or JNK suggesting that the cAMP/PKA pathway is the dominant signaling pathway by which epinephrine enhances BMP activity.

The results of our real-time RT-PCR assay indicating that epinephrine enhanced BMP-2-induced upregulation of the mRNA expression of the osteogenic differentiation markers (ALP, osteocalcin

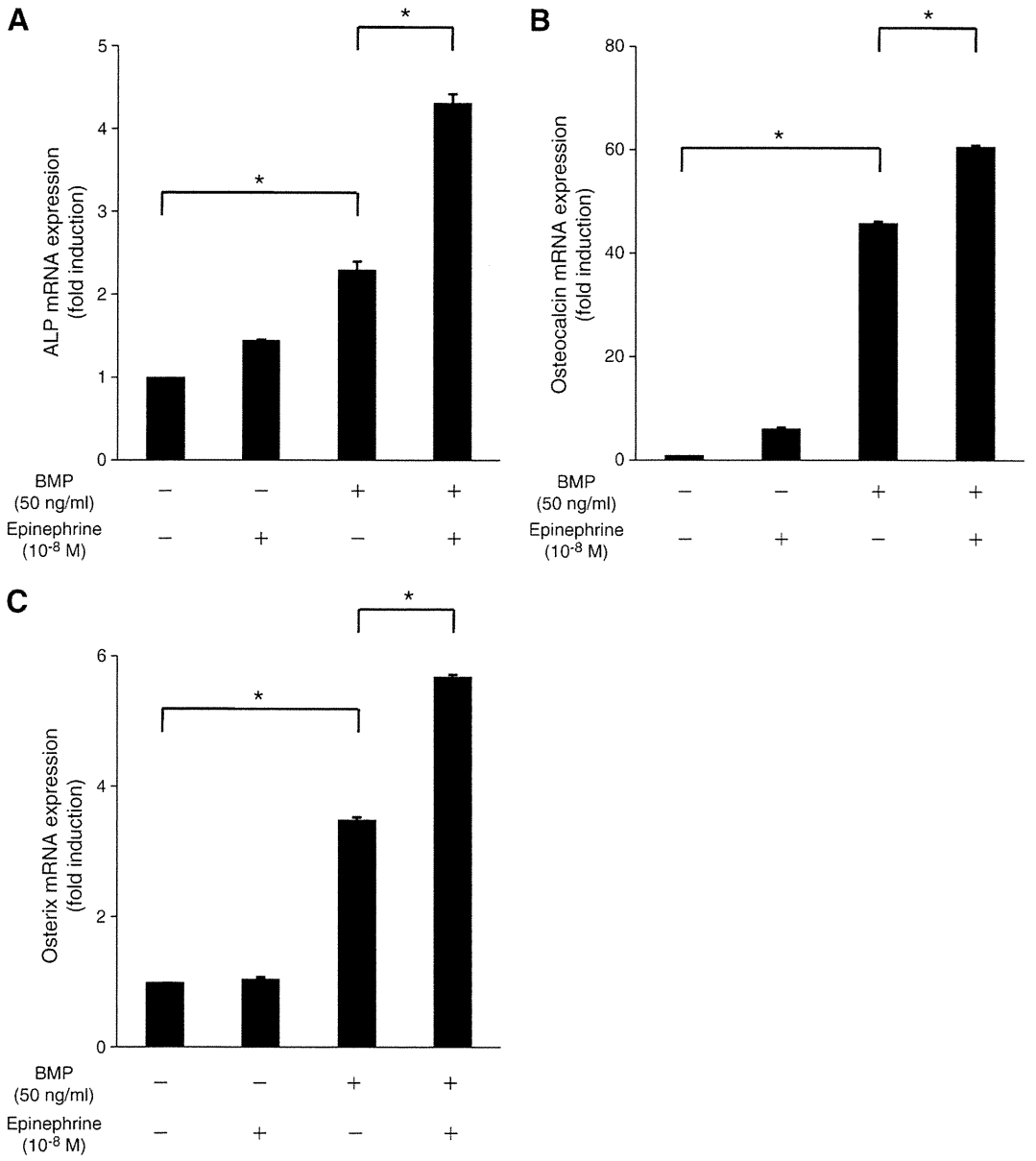

Fig. 7. Effect of epinephrine on BMP-2 induction of the mRNA of ALP, osteocalcin and Osterix. ST2 cells were treated with the indicated concentrations of BMP-2 and/or epinephrine, or with buffer control, following which the mRNA expression of (A) ALP, (B) Osteocalcin or (C) Osterix was assayed on days 3, 6 and 3, respectively, using quantitative RT-PCR. BMP increased the mRNA expression of all three genes and the mRNA expression was further enhanced by epinephrine addition in all cases. Relative mRNA expression was normalized using amplified GAPDH expression values. The bars and lines represent the mean ± SD of 3 wells. BMP: BMP-2 (50 ng/ml), Epinephrine (10^{-8} M): epinephrine (10^{-9} M) added 10 times at 3-min intervals, N.S.: not significant, $^{*}p<0.05$.

and Osterix) suggested that epinephrine might enhance BMP-induced transcriptional activity. This possibility was further suggested by the fact that epinephrine enhanced BMP-induced transcription from a luciferase reporter linked to the Id1 promoter sequence, which is known to be an early response gene in BMP-Smad signaling. Id1 was reported to suppress MyoD (a bHLH type transcriptional factor) function and to shift the differentiation commitment from a myogenic to an osteogenic commitment in response to BMP-2 [42,43]. Therefore, Id1 is an essential gene for BMP-2 induced osteoblastic differentiation. However, the role of Id1 in downstream transcriptional modulation that is required to achieve terminal differentiation into a mature osteoblast has not yet been clarified.

Furthermore, the inability of epinephrine to enhance BMP-2 activation of luciferase expression in experiments using an Id1 promoter with a non-functional mutation in the CRE sequence, suggested that epinephrine enhances BMP-2-evoked transcriptional regulation via CRE. Thus, transcriptional regulator(s) such as CREB or ATF4, that are activated in the cAMP/PKA pathway, and that bind to CRE, might act as enhancers of BRE-mediated transcriptional activity.

Our previous studies indicated that agents that cause elevation of intracellular cAMP, including phosphodiesterase inhibitors (pentoxifylline and rolipram), cell permeable analogues of cAMP (dibutyryl cAMP), a prostaglandin E_2 EP4 agonist (ONO-4819)) and parathyroid hormone (PTH), consistently enhance BMP-2 or BMP-4 action to induce osteoblastic differentiation of mesenchymal cells under *in vivo* and/or *in vitro* conditions [15–20,44–47]. The present study also indicated that epinephrine and other catecholamines are included in this group of agents that are able to promote BMP-induced bone formation through enhancement of the transcriptional activity of BMP-induced intracellular signaling via a common cAMP/PKA/CRE signaling pathway.

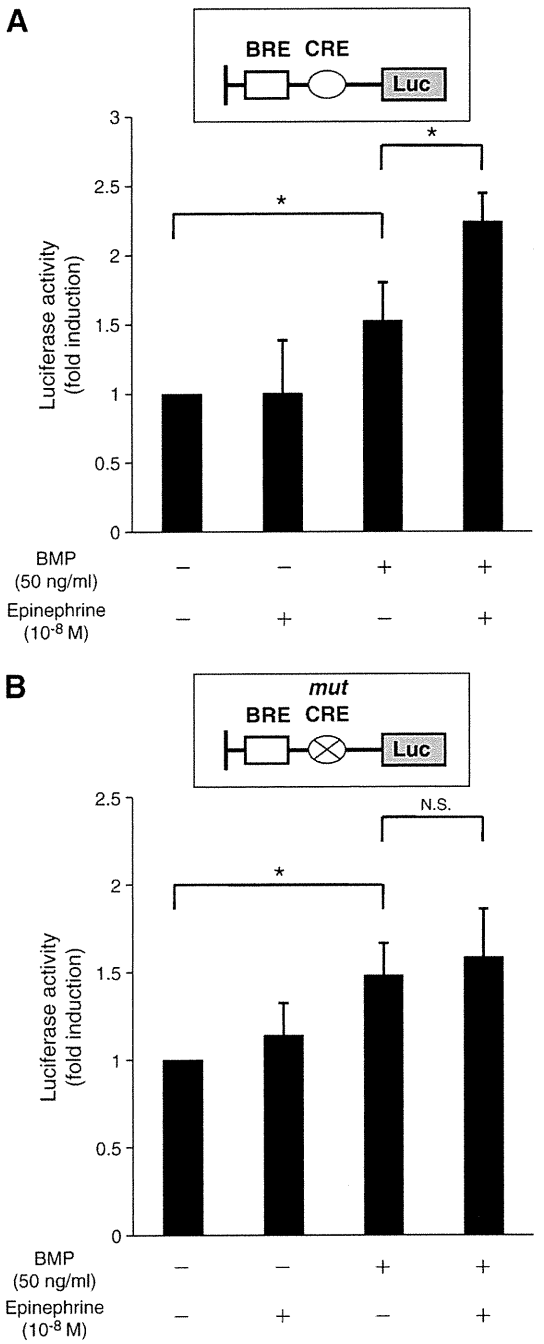

Fig. 8. Effect of epinephrine on BMP-2-induced luciferase activity driven by an Id1 promoter. ST2 cells were transfected with luciferase reporter plasmids driven by the Id1 promoter sequence containing (A) the BRE and CRE elements or (B) containing the BRE and a functionally mutated CRE element. The cells were then treated with the indicated concentrations of BMP-2 and/or epinephrine, or with buffer control, and luciferase activity was assayed after 24 h. BMP-2 enhanced the luciferase activity and this activity was further enhanced by the concurrent addition of epinephrine. The enhancement of BMP-2-induced luciferase activity by epinephrine was abolished when CRE was mutated. The luciferase activity of the control group was assigned a value of 1. The bars and lines represent the mean ± SD of 4 wells. BMP: BMP-2 (50 ng/ml), Epinephrine (10^{-8} M): epinephrine (10^{-9} M) added 10 times at intervals of 3 min, N.S.: not significant, $^{*}p<0.05$. BRE: BMP-responsive element, CRE: cAMP-response element.

Acknowledgments

This work was supported in part by a Grant-in-Aid from the Ministry of Education, Culture, Sports, Science and Technology of Japan (Project Grant No. 20791048).

References

[1] Takeda S, Elefteriou F, Levasseur R, Liu X, Zhao L, Parker K, et al. Leptin regulates bone formation via the sympathetic nervous system. Cell 2002;111:305–17.
[2] Elefteriou F, Ahn J, Takeda S, Starbuck M, Yang X, Liu X, et al. Leptin regulation of bone resorption by the sympathetic nervous system and CART. Nature 2005;434:514–20.
[3] Elmquist J, Strewler G. Physiology: do neural signals remodel bone? Nature 2005;434:447–8.
[4] Sato S, Hanada R, Kimura A, Abe T, Matsumoto T, Iwasaki M, et al. Central control of bone remodeling by neuromedin U. Nat Med 2007;13:1234–40.
[5] Bouxsein M, Devlin M, Glatt V, Dhillon H, Pierroz D, Ferrari S. Mice lacking beta-adrenergic receptors have increased bone mass but are not protected from deleterious skeletal effects of ovariectomy. Endocrinology 2009;150:144–52.
[6] Takeuchi T, Tsuboi T, Arai M, Togari A. Adrenergic stimulation of osteoclastogenesis mediated by expression of osteoclast differentiation factor in MC3T3-E1 osteoblast-like cells. Biochem Pharmacol 2001;61:579–86.
[7] Togari A. Adrenergic regulation of bone metabolism: possible involvement of sympathetic innervation of osteoblastic and osteoclastic cells. Microsc Res Tech 2002;58:77–84.
[8] Arai M, Nagasawa T, Koshihara Y, Yamamoto S, Togari A. Effects of beta-adrenergic agonists on bone-resorbing activity in human osteoclast-like cells. Biochim Biophys Acta 2003;1640:137–42.
[9] Nishiura T, Abe K. Alpha1-adrenergic receptor stimulation induces the expression of receptor activator of nuclear factor kappaB ligand gene via protein kinase C and extracellular signal-regulated kinase pathways in MC3T3-E1 osteoblast-like cells. Arch Oral Biol 2007;52:778–85.
[10] Lipski S. Effects of beta-adrenergic stimulation on bone-marrow function in normal and sublethally irradiated mice. I. The effect of isoproterenol on cAMP content in bone-marrow cells in vivo and in vitro. Int J Radiat Biol Relat Stud Phys Chem Med 1976;29:359–66.
[11] Shultz P, Sedor J, Abboud H. Dopaminergic stimulation of cAMP accumulation in cultured rat mesangial cells. Am J Physiol 1987;253:H358–64.
[12] Kusaka M, Oshima T, Yokota K, Yamamoto S, Kumegawa M. Possible induction of fatty acid cyclooxygenase in mouse osteoblastic cells (MC3T3-E1) by cAMP. Biochim Biophys Acta 1988;972:339–46.
[13] Bjurholm A, Kreicbergs A, Schultzberg M, Lerner U. Neuroendocrine regulation of cyclic AMP formation in osteoblastic cell lines (UMR-106-01, ROS 17/2.8, MC3T3-E1, and Saos-2) and primary bone cells. J Bone Miner Res 1992;7:1011–9.
[14] Moore R, Smith Cn, Bailey C, Voelkel E, Tashjian AJ. Characterization of beta-adrenergic receptors on rat and human osteoblast-like cells and demonstration that beta-receptor agonists can stimulate bone resorption in organ culture. Bone Miner 1993;23:301–15.
[15] Sasaoka R, Terai H, Toyoda H, Imai Y, Sugama R, Takaoka K. A prostanoid receptor EP4 agonist enhances ectopic bone formation induced by recombinant human bone morphogenetic protein-2. Biochem Biophys Res Commun 2004;318:704–9.
[16] Toyoda H, Terai H, Sasaoka R, Oda K, Takaoka K. Augmentation of bone morphogenetic protein-induced bone mass by local delivery of a prostaglandin E EP4 receptor agonist. Bone 2005;37:555–62.
[17] Sugama R, Koike T, Imai Y, Nomura-Furuwatari C, Takaoka K. Bone morphogenetic protein activities are enhanced by 3', 5'-cyclic adenosine monophosphate through suppression of Smad6 expression in osteoprogenitor cells. Bone 2006;38:206–14.
[18] Nakagawa K, Imai Y, Ohta Y, Takaoka K. Prostaglandin E2 EP4 agonist (ONO-4819) accelerates BMP-induced osteoblastic differentiation. Bone 2007;41:543–8.
[19] Ohta Y, Nakagawa K, Imai Y, Katagiri T, Koike T, Takaoka K. Cyclic AMP enhances Smad-mediated BMP signaling through PKA-CREB pathway. J Bone Miner Metab 2008;26:478–84.
[20] Nakao Y, Koike T, Ohta Y, Manaka T, Imai Y, Takaoka K. Parathyroid hormone enhances bone morphogenetic protein activity by increasing intracellular 3', 5'-cyclic adenosine monophosphate accumulation in osteoblastic MC3T3-E1 cells. Bone 2009;44:872–7.
[21] Saito N, Okada T, Horiuchi H, Murakami N, Takahashi J, Nawata M, et al. Biodegradable poly-D,L-lactic acid-polyethylene glycol block copolymers as a BMP delivery system for inducing bone. J Bone Joint Surg Am 2001;83-A(Suppl 1): S92–8.
[22] Kato M, Toyoda H, Namikawa T, Hoshino M, Terai H, Miyamoto S, et al. Optimized use of a biodegradable polymer as a carrier material for the local delivery of recombinant human bone morphogenetic protein-2 (rhBMP-2). Biomaterials 2006;27:2035–41.
[23] Suzuki A, Terai H, Toyoda H, Namikawa T, Yokota Y, Tsunoda T, et al. A biodegradable delivery system for antibiotics and recombinant human bone morphogenetic protein-2: a potential treatment for infected bone defects. J Orthop Res 2006;24:327–32.
[24] Yano K, Hoshino M, Ohta Y, Manaka T, Naka Y, Imai Y, et al. Osteoinductive capacity and heat stability of recombinant human bone morphogenetic protein-2 produced by *Escherichia coli* and dimerized by biochemical processing. J Bone Miner Metab 2009;27:355–63.
[25] Suzuki A, Palmer G, Bonjour J, Caverzasio J. Catecholamines stimulate the proliferation and alkaline phosphatase activity of MC3T3-E1 osteoblast-like cells. Bone 1998;23:197–203.
[26] Nomura-Furuwatari C, Wakitani S, Hashimoto Y, Imai Y, Ohta Y, Nakagawa K, et al. Expression profiles of phosphodiesterase 4D splicing variants in osteoblastic cells. J Bone Miner Metab 2008;26:152–8.
[27] Lai L, Mitchell J. Beta2-adrenergic receptors expressed on murine chondrocytes stimulate cellular growth and inhibit the expression of Indian hedgehog and collagen type X. J Cell Biochem 2008;104:545–53.

[28] Pfaffl M. A new mathematical model for relative quantification in real-time RT-PCR. Nucleic Acids Res 2001;29:e45.
[29] Katagiri T, Imada M, Yanai T, Suda T, Takahashi N, Kamijo R. Identification of a BMP-responsive element in Id1, the gene for inhibition of myogenesis. Genes Cells 2002;7:949–60.
[30] Togari A, Arai M, Mizutani S, Koshihara Y, Nagatsu T. Expression of mRNAs for neuropeptide receptors and beta-adrenergic receptors in human osteoblasts and human osteogenic sarcoma cells. Neurosci Lett 1997;233:125–8.
[31] Kellenberger S, Muller K, Richener H, Bilbe G. Formoterol and isoproterenol induce c-fos gene expression in osteoblast-like cells by activating beta2-adrenergic receptors. Bone 1998;22:471–8.
[32] Summers R, McMartin L. Adrenoceptors and their second messenger systems. J Neurochem 1993;60:10–23.
[33] Takahata Y, Takarada T, Iemata M, Yamamoto T, Nakamura Y, Kodama A, et al. Functional expression of beta2 adrenergic receptors responsible for protection against oxidative stress through promotion of glutathione synthesis after Nrf2 upregulation in undifferentiated mesenchymal C3H10T1/2 stem cells. J Cell Physiol 2009;218:268–75.
[34] Benovic J, Bouvier M, Caron M, Lefkowitz R. Regulation of adenylyl cyclase-coupled beta-adrenergic receptors. Annu Rev Cell Biol 1988;4:405–28.
[35] Bylund D, Eikenberg D, Hieble J, Langer S, Lefkowitz R, Minneman K, et al. International Union of Pharmacology nomenclature of adrenoceptors. Pharmacol Rev 1994;46:121–36.
[36] Zheng M, Zhang S, Zhu W, Ziman B, Kobilka B, Xiao R. beta 2-adrenergic receptor-induced p38 MAPK activation is mediated by protein kinase A rather than by Gi or gbeta gamma in adult mouse cardiomyocytes. J Biol Chem 2000;275:40635–40.
[37] Gong K, Li Z, Xu M, Du J, Lv Z, Zhang Y. A novel protein kinase A-independent, beta-arrestin-1-dependent signaling pathway for p38 mitogen-activated protein kinase activation by beta2-adrenergic receptors. J Biol Chem 2008;283:29028–36.
[38] Suzuki A, Palmer G, Bonjour J, Caverzasio J. Regulation of alkaline phosphatase activity by p38 MAP kinase in response to activation of Gi protein-coupled receptors by epinephrine in osteoblast-like cells. Endocrinology 1999;140:3177–82.
[39] Magne S, Couchie D, Pecker F, Pavoine C. Beta(2)-adrenergic receptor agonists increase intracellular free Ca(2+) concentration cycling in ventricular cardiomyocytes through p38 and p42/44 MAPK-mediated cytosolic phospholipase A(2) activation. J Biol Chem 2001;276:39539–48.
[40] Frost R, Nystrom G, Lang C. Epinephrine stimulates IL-6 expression in skeletal muscle and C2C12 myoblasts: role of c-Jun NH2-terminal kinase and histone deacetylase activity. Am J Physiol Endocrinol Metab 2004;286:E809–17.
[41] Yamauchi J, Hirasawa A, Miyamoto Y, Itoh H, Tsujimoto G. Beta2-adrenergic receptor/cyclic adenosine monophosphate (cAMP) leads to JNK activation through Rho family small GTPases. Biochem Biophys Res Commun 2001;284:1199–203.
[42] Katagiri T, Akiyama S, Namiki M, Komaki M, Yamaguchi A, Rosen V, et al. Bone morphogenetic protein-2 inhibits terminal differentiation of myogenic cells by suppressing the transcriptional activity of MyoD and myogenin. Exp Cell Res 1997;230:342–51.
[43] López-Rovira T, Chalaux E, Massagué J, Rosa J, Ventura F. Direct binding of Smad1 and Smad4 to two distinct motifs mediates bone morphogenetic protein-specific transcriptional activation of Id1 gene. J Biol Chem 2002;277:3176–85.
[44] Kinoshita T, Kobayashi S, Ebara S, Yoshimura Y, Horiuchi H, Tsutsumimoto T, et al. Phosphodiesterase inhibitors, pentoxifylline and rolipram, increase bone mass mainly by promoting bone formation in normal mice. Bone 2000;27:811–7.
[45] Horiuchi H, Saito N, Kinoshita T, Wakabayashi S, Yotsumoto N, Takaoka K. Effect of phosphodiesterase inhibitor-4, rolipram, on new bone formations by recombinant human bone morphogenetic protein-2. Bone 2002;30:589–93.
[46] Tsutsumimoto T, Wakabayashi S, Kinoshita T, Horiuchi H, Takaoka K. A phosphodiesterase inhibitor, pentoxifylline, enhances the bone morphogenetic protein-4 (BMP-4)-dependent differentiation of osteoprogenitor cells. Bone 2002;31:396–401.
[47] Wakabayashi S, Tsutsumimoto T, Kawasaki S, Kinoshita T, Horiuchi H, Takaoka K. Involvement of phosphodiesterase isozymes in osteoblastic differentiation. J Bone Miner Res 2002;17:249–56.

J Neurosurg Spine 13:758–765, 2010

The influence of approach side on facet preservation in microscopic bilateral decompression via a unilateral approach for degenerative lumbar scoliosis

Clinical article

Akira Matsumura, M.D., Takashi Namikawa, M.D., Hidetomi Terai, M.D., Tadao Tsujio, M.D., Akinobu Suzuki, M.D., Sho Dozono, M.D., Hiroyuki Yasuda, M.D., and Hiroaki Nakamura, M.D.

Department of Orthopaedic Surgery, Osaka City University Graduate School of Medicine, Osaka City, Japan

Object. The authors compared the clinical outcomes of microscopic bilateral decompression via a unilateral approach (MBDU) for the treatment of degenerative lumbar scoliosis (DLS) and for lumbar canal stenosis (LCS) without instability. The authors also compared postoperative spinal instability in terms of different approach sides (concave or convex) following the procedure.

Methods. The authors retrospectively reviewed data obtained in 50 consecutive patients (25 in the DLS group and 25 in the LCS group) who underwent MBDU; the minimum follow-up period was 2 years. Patients with DLS were divided into 2 subgroups according to the surgical approach side: a concave group (23 segment) and a convex group (17 segments). The Japanese Orthopaedic Association Scale scores for the assessment of low-back pain were evaluated before surgery and at final follow-up. The Japanese Orthopaedic Association Scale scores and recovery rates were compared between the DLS and LCS groups, and between the convex and concave groups. Cobb angle and scoliotic wedging angle (SWA) were evaluated on standing radiographs before surgery and at final follow-up. Facet joint preservation (the percentage of preservation) was assessed on pre- and postoperative CT scans, compared between the LCS and DLS groups, and compared between the concave and convex groups. The influence of approach side on postoperative progression of segmental instability was also examined in the DLS group.

Results. The mean recovery rate was 58.7% in the DLS and 62.0% in the LCS group. The mean recovery rate was 58.6% in the convex group and 60.6% in the concave group. There were no significant differences in recovery rates between the LCS and DLS groups, or between the DLS subgroups. The mean Cobb angles in the DLS group were significantly increased from 12.7° preoperatively to 14.1° postoperatively ($p < 0.05$), and mean preoperative SWAs increased significantly from 6.2° at L3–4 and 4.1° at L4–5 preoperatively to 7.4° and 4.9°, respectively, at final follow-up ($p < 0.05$). There was no significant difference in percentage of preservation between the DLS and LCS groups. The mean percentages of preservation on the approach side in the DLS group at L3–4 and L4–5 were 89.0% and 83.1% in the convex group, and those in the concave group were 67.3% and 77.6%, respectively. The percentage of preservation at L3–4 was significantly higher in the convex than the concave group. The mean SWA had increased in the concave group ($p = 0.01$) but not the convex group ($p = 0.15$) at final follow-up.

Conclusions. The MBDU can reduce postoperative segmental spinal instability and achieve good postoperative clinical outcomes in patients with DLS. The convex approach provides surgeons with good visibility and improves preservation of facet joints. *(DOI: 10.3171/2010.5.SPINE091001)*

Key Words • **microscopic decompression** • **unilateral approach** • **degenerative lumbar scoliosis** • **facet joint preservation** • **postoperative instability**

Lumbar spinal canal stenosis combined with scoliosis is often seen in elderly patients. The patients suffer from low-back pain, radiating leg pain, and intermittent claudication. Conservative therapy may not be adequate, and some form of surgical intervention is generally indicated. The choice of surgical method depends on the magnitude of the curvature, spinal instability, and the symptoms. Simmons[18] classified 2 types of adult scoliosis, depending on the presence or absence of preexisting scoliosis. Aebi[2] classified 4 types scoliosis based on the origin. These 2 authors recommended corrective surgery for degenerative adult scoliosis when

Abbreviations used in this paper: AP = anteroposterior; DLS = degenerative lumbar scoliosis; JOA = Japanese Orthopaedic Association; LCS = lumbar spinal canal stenosis; MBDU = microscopic bilateral decompression via a unilateral approach; SWA = scoliotic wedging angle.

the disease was idiopathic and decompression and fusion surgery when the scoliosis was degenerative (de novo) in nature.[2,18] The surgical aims differ between these 2 types of scoliosis: corrective surgery aims to improve spinal balance, whereas decompression and short fusion aims to relieve neurological symptoms. However, the indications for surgery and definition of the fusion area have not been established. In addition, DLS is seen predominantly in the elderly population, and elderly patients usually have more medical comorbidities, such as hypertension, diabetes, and cardiopulmonary disease.[14] Furthermore, osteoporosis in the elderly makes spinal implants difficult to anchor, even with a pedicle screw fixation system.[2,4] Patients with DLS usually require long-segment fusion, which can increase the risk instrumentation-related complications. Surgery for degenerative adult scoliosis can result in significant complications, including pseudarthrosis, adjacent-segment disease, neurological deficits, cardiopulmonary disease, deep vein thrombosis, and wound infection. The incidence of complications reported in most series has been high, ranging from 20% to 80%.[2,3]

Preservation of the posterior elements is the most important factor in the success of decompression surgery for LCS.[1,5,10,17] Decompressive laminectomy is one of the most common surgical procedures for LCS, and some authors have reported good clinical outcomes after laminectomy.[7,21] However, despite affording a wide decompression, laminectomy or "unroofing" of the spinal canal, can cause destruction or impairment insufficiency of the pars interarticularis or facet joints, resulting in segmental instability and paravertebral muscle atrophy.[3,17] Some authors have recently reported good clinical outcomes following minimally invasive decompression in which the posterior elements, such as the paravertebral muscle, facet joints, and lamina, have been preserved.[6,8,19] Good clinical outcomes in patients with LCS have also been reported for MBDU, which was initially described by Young et al.[23] in 1988 and was later modified by Weiner et al.[20] Additionally, a few authors have reported the clinical results of MBDU for LCS in cases involving mild instability, such as spondylolisthesis[15] and hemodialysis.[16] However, there have been few reports regarding the clinical outcome after decompression for DLS. We initiated the use of the MBDU for DLS in an attempt to reduce postoperative instability. In the present study we compared the clinical outcomes of MBDU for DLS and for LCS without instability. The postoperative instability following concave- or convex-side approaches during MBDU for DLS were also compared.

Methods

The authors retrospectively reviewed data obtained in 50 consecutive patients with LCS who underwent MBDU; the minimum follow-up period was 2 years. The patients were divided into 2 groups, according to the nature of the spinal deformity: 25 patients with DLS group and and 25 patients with LCS without spinal deformity. The mean age in the DLS group was 69.6 years (range 53–82 years), and there were 10 men and 15 women; the mean age in the LCS group was 70.1 years (range 54–84 years), and there were 15 men and 10 women. The mean follow-up duration 43.6 months (range 24–89 months) in the DLS group and 42.1 months (range 24–79 months) in the LCS group. There were no significant intergroup differences in terms of the aforementioned parameters ($p > 0.05$). Decompression was performed at a single level in 10 cases in the DLS group and 6 cases in the LCS group; at 2 levels in 10 in the DLS group and in 11 cases in the LCS group, and at 3 levels in 5 cases in the DLS group and in 6 cases in the LCS group. Demographic and disease-related data are summarized in Table 1. Surgery was performed at L3–4 (18 segments), L4–5 (22 segments), and at other levels (5 segments) in the DLS group, and at L3–4 (16 segments), L4–5 (23 segments), and at other levels (11 segments) in the LCS group. We radiographically evaluated the L3–4 and L4–5 levels in both groups (40 in the DLS group and 39 in the LCS group [having excluding "other levels" from the analysis of both groups]). We divided the decompression levels in the DLS group into 2 subgroups according to the approach side of the surgery: from the concave side (23 segments) and from the convex side (17 segments). Details of the decompression segments are shown in Table 2. The following clinical and radiographic records were available for all patients: medical charts, standing AP and lateral radiographs obtained preoperatively and at least 2 years after surgery, and preoperative and postoperative CT scans.

Surgical Decision Making

Patients in whom the Cobb angle exceeded 10° in the coronal plane were considered to have DLS. Curvatures in all patients were classified as de novo scoliosis. Patients with spondylolisthesis and spondylolysis were excluded from the LCS group. Patients from both groups with neurogenic intermittent claudication (radiculopathy or cauda equina syndrome), and with no response to conservative therapy over at least 3 months, were considered to be suitable to undergo MBDU. Lumbar canal stenosis was confirmed by MR imaging, myelography, and CT myelography. Exclusion criteria for MBDU in patients with DLS were as follows: 1) Cobb angle greater than 25°, 2) severe low-back pain, 3) changes in segmental disc wedging between standing and prone position greater

TABLE 1: Summary of demographic and disease-related data

Characteristic	DLS Group	LCS Group	p Value
no. of patients	25	25	
male/female ratio	10:15	15:10	0.041
age (yrs)			
mean	69.6	70.1	0.82
range	53–82	54–84	
follow-up (mos)			
mean	43.6	42.1	0.76
range	24–89	24–79	
no. of decompression levels			0.17
1	10	6	
2	10	11	
3	5	6	
total	45	50	

TABLE 2: Decompression segments in 2 groups*

Variable	DLS Group	LCS Group	p Value
decompression level			0.17
L3–4†	18	16	
L4–5†	22	23	
others	5	11	
approach side‡			
concave	23	NA	
convex	17	NA	

* NA = not applicable.
† Radiographic data were only evaluated at the L3–4 and L4–5 segments in each group.
‡ The DLS group was divided into 2 subgroups, according to the approach side at surgery.

than 5°, 4) lateral disc slippage greater than 3 mm, and 5) foraminal stenosis needing more than 50% facetectomy for decompression.

Surgical Procedures

An approximately 35-mm midline incision for 1-level decompression (for example, at L4–5) was made to unilaterally expose the posterior elements lateral to the facet joints. Using a high-speed drill (with a 3- or 4-mm diamond-tipped bur) and a microscope, we removed the L-4 lamina cranially to the attachment of the ligamentum flavum, only minimally resecting the medial part of the L4–5 facet joint. The L-5 lamina was removed caudally to the attachment of the ligamentum flavum. Using a Kerrison rongeur and microcurette, the medial, cranial, and caudal margins of the ligamentum flavum were freed. The contralateral side was then approached. With the operating table rotated approximately 25° degree to the contralateral side, the L-4 spinous process was undercut, and the deeper portion of the interspinous ligament was removed to visualize the posterior surface of the contralateral ligamentum flavum. The caudal portion of the L-4 inner lamina and cranial part of the L-5 inner lamina were then partially removed using a high-speed drill to expose the whole ligamentum flavum. The contralateral facet was trimmed using the high-speed drill, and the attachment of the facet portion of the ligamentum flavum was detached using a microcurette or Kerrison rongeur. Finally, the ligamentum flavum was removed in 1 or 2 pieces. Decompression of the bilateral nerve roots was then evaluated.

Clinical Evaluation

The JOA score for assessment of low-back pain was evaluated before surgery and at final follow-up. The JOA score comprises 9 points assigned for subjective symptoms, 6 points for clinical signs, and 14 points for the restriction of activities of daily living, giving a total score of 29 points (Table 3).[22] The recovery rate was calculated as follows: (postoperative JOA score – preoperative JOA score)/(29 – preoperative JOA score) × 100(%).[3] We compared the JOA Scale scores and recovery rates between the DLS and LCS groups, as well as between the convex and concave groups.

Radiographic Evaluation

The Cobb angle and SWA were evaluated radiographically on standing radiographs before surgery and at final follow-up (Fig. 1). Facet joint preservation was evaluated on CT scans. The length of the facet joint was measured using Scion Image software, and the percentage of facet preservation was calculated using the equation: percentage of preserved facet = the length of the postoperative facet (b)/the length of the preoperative facet (a) × 100 (Fig. 2). The percentage of preserved facet was compared between the LCS and DLS groups, as well as between the concave and convex groups. We also analyzed the influence of the approach side on postoperative progression of segmental instability in the DLS group.

Statistical Analysis

All data were analyzed statistically using the ANOVA, Mann-Whitney U-test, paired t-test, or unpaired t-test, as

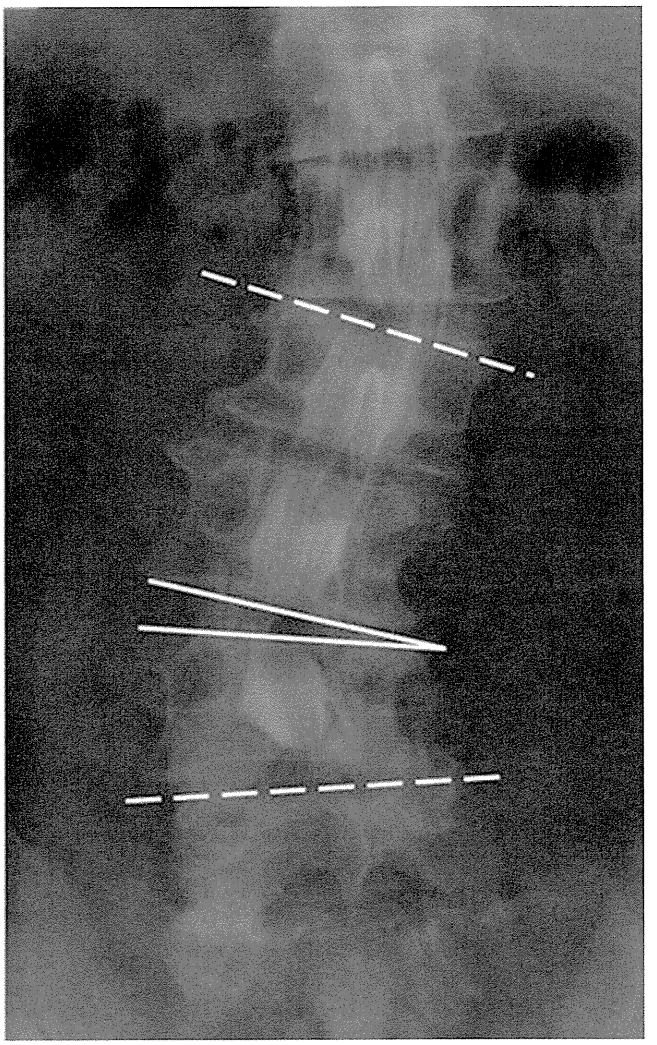

FIG. 1. Radiographic parameters. *Dotted lines* indicate Cobb angle and *solid lines* indicate scoliotic wedging angle.

TABLE 3: Summary of the JOA scoring system for treatment of low-back pain*

Factor	Item	Description	Score
subjective symptoms	low-back pain (3 points)	none	3
		occasional mild pain	2
		frequent mild or occasional severe pain	1
		continuous severe pain	0
	leg pain &/or tingling (3 points)	none	3
		occasional mild symptoms	2
		frequent mild or occasional severe symptoms	1
		continuous severe symptoms	0
	gait (3 points)	normal	3
		able to walk farther than 500 m although results in pain, tingling, &/or muscle weakness	2
		unable to walk farther than 500 m, results in pain, tingling, &/or muscle weakness	1
		unable to walk farther than 100 m, results in pain, tingling, &/or muscle weakness	0
objective symptoms	straight leg–raising test (2 points)	normal	2
		30–70°	1
		<30°	0
	sensory abnormality (2 points)	normal	2
		mild disturbance (not subjective)	1
		marked disturbance	0
	motor disturbance (MMT) (2 points)	normal (Grade 5)	2
		slight weakness (Grade 4)	1
		marked weakness (Grade 3–0)	0
restriction of ADLs (14 points)	turning over while lying standing washing leaning forward sitting (about 1 hr) lifting or holding heavy objects walking	no restriction moderate restriction severe restriction	2 1 0
urinary bladder function (−6 points)		normal	0
		mild dysuria	−3
		severe dysuria	−6
total score			29

* The Hirabayashi method is used to determine a patient's recovery rate: recovery rate = (final score – preoperative score) / (29 − preoperative score) × 100%. Abbreviation: ADLs = activities of daily living.

appropriate. The level of significance for all tests was defined as $p < 0.05$.

Results

Clinical Outcome

The mean JOA scores in the DLS and LCS groups were 11.2 and 12.5 before surgery and 21.6 and 22.5 at the final follow-up, respectively (Fig. 3 upper). The mean recovery rate was 58.7% in the DLS group and 62.0% in the LCS group; there was no significant difference in recovery rate between groups ($p = 0.49$). The JOA scores in the concave and convex groups were 10.7 and 11.5 before surgery and 21.8 and 21.8 at the final follow-up, respectively (Fig. 3 lower). The mean recovery rate was 58.6% in the convex and 60.6% in the concave group; there was no significant difference in recovery rates between the convex and concave groups ($p = 0.89$).

Radiographic Evaluation

The mean Cobb angles in the DLS group increased significantly from 12.7° preoperatively to 14.1° at final follow-up ($p = 0.0009$). The mean SWAs at L3–4 and L4–5 increased significantly from 6.2° and 4.1° preoperatively to 7.4° and 4.9° at final follow-up, respectively ($p = 0.05$ and 0.003, respectively). These data are summarized in Table 4.

The mean percentages of facet preservation in the LCS group were 73.4% on the approach side and 95.0% on the contralateral side at L3–4; they were 85.1% on the approach side and 95.9% on the contralateral side at

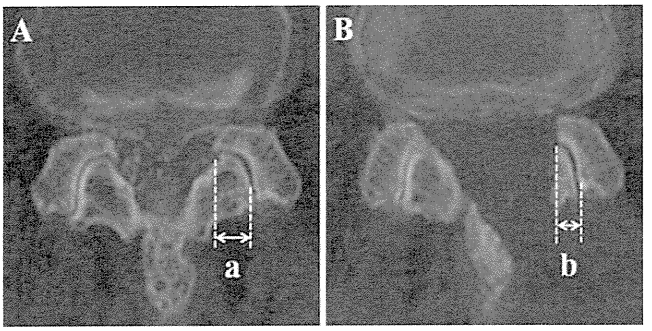

FIG. 2. Measurement of facet joint preservation on preoperative **(A)** and at final follow-up **(B)** CT scans. The length of the facet joint was measured using Scion Image software, and the percentage of facet preservation was calculated using the following equation: (percentage of facet preservation) = b/a × 100.

L4–5. The mean percentages of facet preservation in the DLS group were 79.4% on the approach side and 97.3% on the contralateral side at L3–4; they were 80.8% on the approach side and 96.1% on the contralateral side at L4–5. There was no significant difference between the DLS and LCS groups (Fig. 4 upper). The percentage of facet preservation was only compared between the convex and concave groups on the approach side. The mean percentages of facet preservation at L3–4 and L4–5 were 89.0% and 83.1% in the convex group and 67.3% and 77.6% in the concave group, respectively. The percentage of preserved facet was significantly higher in the convex group than the concave group at L3–4 (p = 0.003, Fig. 4 lower). The mean SWA in the concave group, but not in the convex group, was significantly increased at final

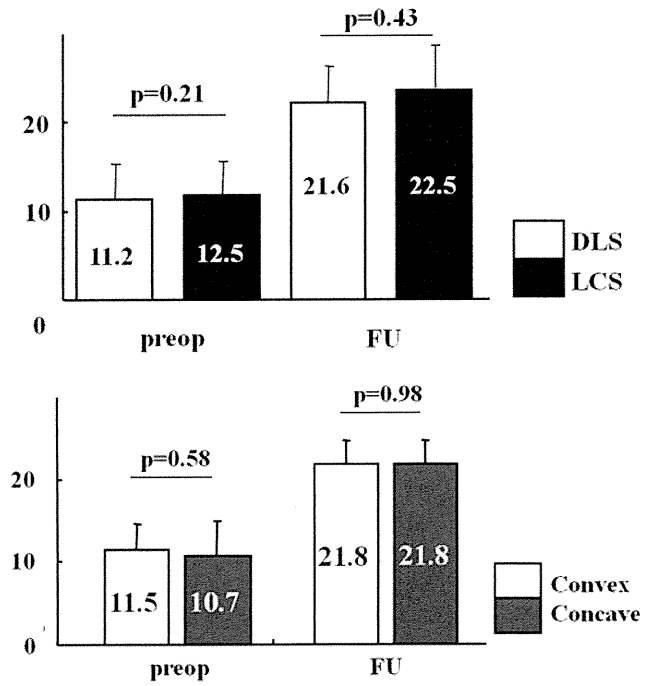

FIG. 3. **Upper:** Mean JOA Scale scores in the DLS and LCS groups; there was no significant difference between the groups. **Lower:** Mean JOA Scale scores in the convex and concave groups; there was no significant difference between groups. FU = final follow-up.

TABLE 4: Radiographic evaluation in DLS group*

Angle (°)	Preop	Follow-Up	p Value
Cobb angle	12.7 ± 3.2	14.1 ± 4.3	0.0009
SWA			
L3–4	6.2 ± 3.1	7.4 ± 3.9	0.05
L4–5	4.1 ± 2.6	4.9 ± 2.7	0.003

* Data presented as the mean ± SD and were analyzed using paired t-tests.

follow-up (p = 0.01 and 0.15, respectively; Table 5). The radiographic studies of both DLS subgroups are shown in Figs. 5 and 6. The facet joint on the approach side could be preserved using the convex approach, and the latest radiographs showed no obvious curve progression (Fig. 5). In contrast, poor facet preservation on the approach side with the concave approach led to curve progression and poor clinical outcome (Fig. 6).

Revision Surgery

Because of residual leg pain and low-back pain, 2 patients in the DLS group underwent additional fusion surgery during the follow-up period. Both patients underwent L3–4 and L4–5 MBDU via the concave approach. One patient complained of a recurrence of leg pain and severe low-back pain 6 months after initial surgery. A CT scan showed that the percentage of facet preservation on the concave side was 56%, and a radiograph showed that

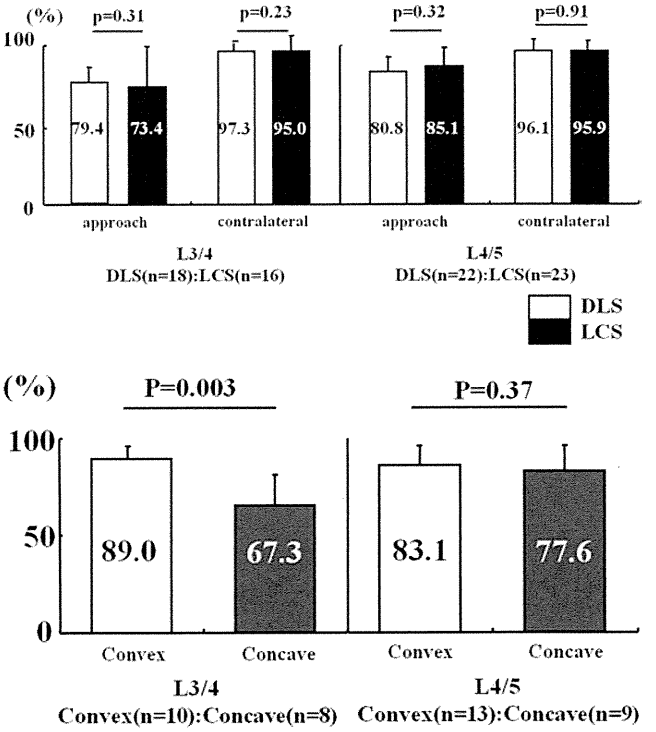

FIG. 4. **Upper:** Mean percentage of facet preservation in the DLS and LCS groups; there was no significant difference between groups. **Lower:** Mean percentage of facet preservation on the approach side in the degenerative lumbar scoliosis group. The percentage of preserved facet was significantly higher in the convex than in the concave group at L3–4 level (p = 0.003). n = number of treated segments.

TABLE 5: Differences in SWAs between convex and concave groups*

SWA (°)	Preop	Follow-Up	p Value
convex	5.41 ± 2.90	5.96 ± 3.52	0.15
concave	4.98 ± 3.19	6.10 ± 3.57	0.01

* Concave and convex indicate approach side of MBDU. Data are presented as the mean ± SD were analyzed using paired t-tests.

the SWA at L4–5 had progressed from 9° before surgery to 13° at revision surgery. The other patient complained of recurrent leg pain 1 year after initial surgery. Radiography and MR imaging showed L5–S1 foraminal stenosis. A huge osteophyte originating from the L5–S1 endplate compressed the L-5 nerve root anteriorly, and L5–S1 transforaminal lumbar interbody fusion was therefore performed.

Discussion

Degenerative lumbar scoliosis can be divided into 2 main types: degenerative scoliosis in conjunction with idiopathic scoliosis, and degenerative scoliosis with no previous scoliosis (de novo scoliosis).[2,18] Surgeons choose the surgical procedure based on the magnitude of the patient's spinal deformity, symptoms, and general condition. Decompressive surgery without fusion can sometimes result in good outcomes in patients with mild DLS, but some surgeons are concerned that in patients with DLS decompression can result in postsurgical spinal instability. The most important factor in the success of decompression for LCS is the preservation of the posterior elements. Decompressive laminectomy and bilateral unroofing can allow for a wide decompression, and acceptable clinical results have been reported in patients with radiculopathy or neurogenic claudication.[7,21] However, destruction or impairment of the pars interarticularis or facet joints can lead to postoperative spinal instability.[3] Additionally, a laminectomy requires wide paravertebral muscle stripping from the lamina, which can potentially denervate the paravertebral muscles and cause subsequent atrophy—changes that have been correlated with postoperative failed–back surgery syndrome.[17] Indications for decompressive laminectomy are therefore limited in patients with LCS when spinal instability is absent. An MBDU is a minimally invasive technique used to treat LCS.[20,23] It achieves good decompression without injuring the supra- or interspinous ligament complexes or contralateral paraspinal muscles, and it minimizes postoperative spinal instability. The present study demonstrated, in a minimum follow-up period of 2 years, a mean recovery rate of 58.7% following MBDU for DLS, which was equivalent to the recovery rate for LCS. Some authors recently presented a new minimally invasive decompression technique for LCS without spinal instability and demonstrated a recovery rate of approximately 60% (range 61%–67%).[6,8,19] Our recovery rate was similar to this and is thus considered to be acceptable. The Cobb angle and SWA were significantly increased at final follow-up, but the curve and disc wedging only increased by 0.5° in 1 year, and the progression in postoperative instability was therefore also deemed acceptable.[11] Although this study has certain limitations, in that MBDU was not indicated in all patients with DLS, DLS with mild segmental instability and mild spinal deformity was thought to be a good indication for this procedure.

The etiology of DLS is thought to involve asymmetrical disc degeneration leading to disc wedging and facet joint incongruity.[12,13] The facet joints thus play an important role in spinal stability, especially in DLS. A biomechanical study clearly showed that the amount of preserved facet joint influenced segmental spinal stability.[1] In the present study we found that the percentage of

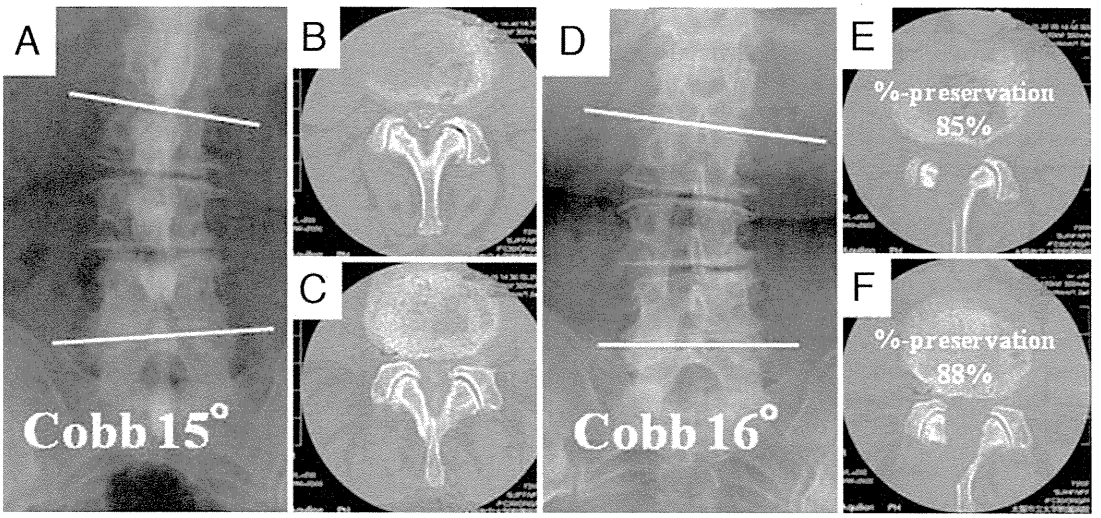

Fig. 5. Imaging studies obtained in a 74-year-old woman who underwent MBDU from the convex side. Preoperative standing AP radiograph **(A)** and preoperative axial CT scans of the L3–4 level **(B)** and L4–5 level **(C)**. The spinous processes are inclined to the contralateral side, providing a wider view from the convex than the concave side. Postoperative AP radiograph **(D)** after 5 years demonstrating no obvious postoperative spinal instability. Postoperative axial CT images at L3–4 **(E)** and L4–5 **(F)** revealing good preservation of the facet joints (percentage of facet preservation [%-preservation] on the approach side: L3–4, 85%; L4–5, 88%).

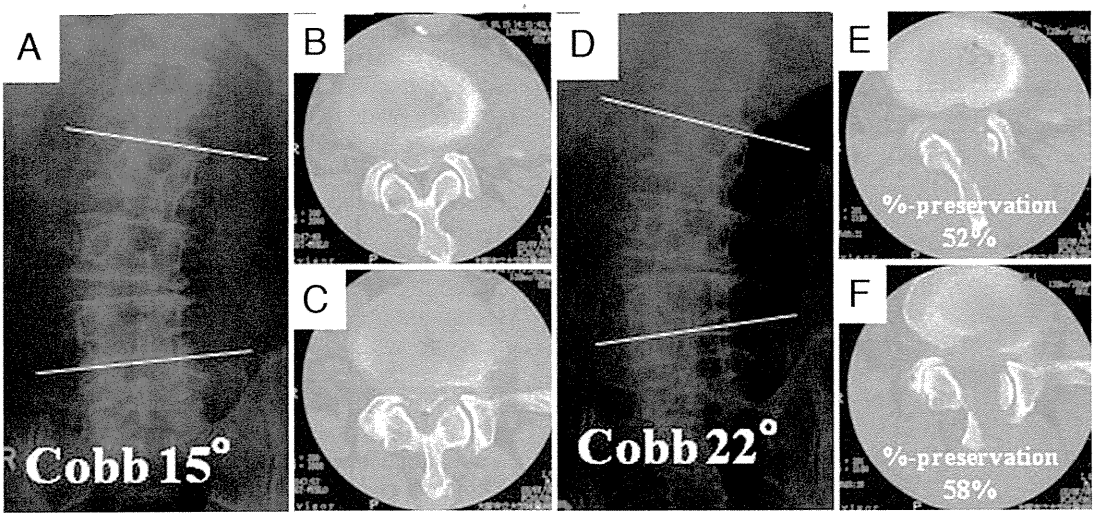

Fig. 6. Imaging studies acquired in a 71-year-old man who underwent MBDU on the concave side. Preoperative standing AP radiograph **(A)**, preoperative axial CT images at L3–4 **(B)** and L4–5 **(C)**. The spinous processes are inclined to the approach side, giving a narrower view from the concave side. Postoperative AP radiograph **(D)** acquired 2 years postoperatively demonstrating obvious postoperative spinal instability. Postoperative axial CT images at L3–4 **(E)** and L4–5 **(F)** showing poor preservation of the facet joints (percentage of facet preservation on the approach side: L3–4, 52%; L4–5, 58%).

facet preservation in the DLS group was approximately 80% on the approach side and 95% on the contralateral side, values that did not differ significantly from those in the LCS group. In DLS, spinal stenosis is often more severe on the concave than the convex side, and the concave side appears to be the symptomatic side.[9] We therefore tended to select the concave side as the approach side. However, the percentage preserved facet on the approach side was greater than that on the contralateral side. The poorer facet preservation on the approach side means that the approach-side effect must be taken into consideration when performing MBDU for DLS. Comparison of the preservation between the concave and convex approaches clearly showed that latter achieved significantly better facet preservation than the concave approach, because the spinous process tended to incline to the concave side due to of the vertebral rotation. The spinous process inclined to the contralateral side, providing a wider view from the convex in DLS. A wider view enables the surgeon to preserve the facet joint during surgery. Although there was no significant difference in recovery rates between the 2 groups, the SWA significantly increased only in the concave group. Additionally, the vertebra inclines to the concave side and then translates laterally. Thus, the facet joint on the concave side is more important than that on the convex side for stabilizing segmental instability. These results suggest that the convex approach should be preferred over the concave approach when performing MBDU in patients with DLS.

Conclusions

Unilateral-approach MBD can achieve good clinical outcomes in patients with DLS during a follow-up period exceeding 2 years. Additionally, it can reduce postoperative segmental spinal instability. A convex approach for MBD in patients with DLS allows good visualization, thus enabling surgeons to preserve the facet joints.

Disclosure

The authors report no conflict of interest concerning the materials or methods used in this study or the findings specified in this paper.

Author contributions to the study and manuscript preparation include the following. Conception and design: Matsumura, Namikawa. Acquisition of data: Matsumura, Namikawa, Terai, Tsujio, Suzuki. Analysis and interpretation of data: Matsumura, Namikawa, Dozono, Yasuda. Drafting the article: Matsumura, Nakamura. Critically revising the article: Matsumura. Reviewed final version of the manuscript and approved it for submission: all authors. Statistical analysis: Matsumura. Administrative/technical/material support: Matsumura. Study supervision: Matsumura, Nakamura.

References

1. Abumi K, Panjabi MM, Kramer KM, Duranceau J, Oxland T, Crisco JJ: Biomechanical evaluation of lumbar spinal stability after graded facetectomies. **Spine 15:**1142–1147, 1990
2. Aebi M: The adult scoliosis. **Eur Spine J 14:**925–948, 2005
3. Bresnahan L, Ogden AT, Natarajan RN, Fessler RG: A biomechanical evaluation of graded posterior element removal for treatment of lumbar stenosis: comparison of a minimally invasive approach with two standard laminectomy techniques. **Spine 34:**17–23, 2009
4. Cho KJ, Suk SI, Park SR, Kim JH, Kim SS, Choi WK, et al: Complications in posterior fusion and instrumentation for degenerative lumbar scoliosis. **Spine 32:**2232–2237, 2007
5. Goel VK, Fromknecht SJ, Nishiyama K, Weinstein J, Liu YK: The role of lumbar spinal elements in flexion. **Spine 10:**516–523, 1985
6. Hatta Y, Shiraishi T, Sakamoto A, Yato Y, Harada T, Mikami Y, et al: Muscle-preserving interlaminar decompression for the lumbar spine: a minimally invasive new procedure for lumbar spinal canal stenosis. **Spine 34:**E276–E280, 2009
7. Iguchi T, Kurihara A, Nakayama J, Sato K, Kurosaka M, Yamasaki K: Minimum 10-year outcome of decompressive laminectomy for degenerative lumbar spinal stenosis. **Spine 25:** 1754–1759, 2000
8. Ikuta K, Arima J, Tanaka T, Oga M, Nakano S, Sasaki K, et al: Short-term results of microendoscopic posterior decompression for lumbar spinal stenosis. Technical note. **J Neurosurg Spine 2:**624–633, 2005